Electronic Supplementary Material (ESI) for Journal of Materials Chemistry C.
This journal is © The Royal Society of Chemistry 2022

Electronic Supplementary Information

Achieving redox-responsive organic afterglow via dopant-matrix design strategy

*Xuefeng Chen,[#] Guangming Wang,[#] Xiuzheng Chen, Xinjian Deng and Kaka Zhang**

Key Laboratory of Synthetic and Self-Assembly Chemistry for Organic Functional Molecules, Shanghai Institute of Organic Chemistry, University of Chinese Academy of Sciences, Chinese Academy of Sciences, 345 Lingling Road, Shanghai 200032, People's Republic of China.

*Email: zhangkaka@sioc.ac.cn

Table of Contents

Experimental Contents

Experimental Contents

Materials

Phenyl ether (>99.0%, Aladdin), 9,9-dimethyl fluorene (98%, Adamas), 9,9-diphenylfluorene (98%, ARK), 9,9′-spirobifluorene (98%, Bide Pharmatech), acetic anhydride (98.5%, Sinopharm Chemical Reagent), boron trifluoride diethyl etherate (98%, TCI), NaClO (reagent, 5%chlorine, Acros), triphenylphosphine (>99.0%, Adamas), triphenylphosphine oxide (98%, Aladdin).

Synthesis of $DPEBF_2$ via cascade reaction

Into a round bottom flask were added phenyl ether (0.2 mL, 1.3 mmol), acetic anhydride (2 mL) and boron trifluoride diethyl etherate (0.8 mL). The reaction mixture was heated to 60 °C and stirred for 4 h. Then the reaction was quenched by adding the reaction mixture drop wise into cold water. The precipitates were washed by water for three times and dried under vacuum. The crude product was purified by column chromatography over silica gel using petroleum ether/dichloromethane (1:1) as eluent to give white solids with an isolation yield of 32%. The $DPEBF_2$ was further purified by three cycles of recrystallization in spectroscopic grade dichloromethane/hexane (CCDC 2159995). ^{1}H NMR (400 MHz, Chloroform-*d,* relative to Me_4Si/ppm) δ 8.05 (d, *J* = 2.4 Hz, 1H), 8.03 (d, *J* = 2.2 Hz, 1H), 7.44 (t, *J* = 7.9 Hz, 2H), 7.28 (t, *J* = 6.0 Hz 1H), 7.10 (d, *J* = 8.3 Hz, 2H), 7.04 (d, *J* = 9.0 Hz, 2H), 6.48 (s, 1H), 2.39 (s, 3H). ^{13}C NMR (100 MHz, Chloroform-*d*) δ 191.05, 181.79, 164.54, 154.58, 131.64, 130.30, 125.43, 124.93, 120.63, 117.51, 96.67, 24.64.^{19}F NMR (376 MHz, Chloroform-*d*, 298 K, relative to $CFCl_3$ /ppm) δ -139.33 (20%), -139.39 (80%). ^{11}B NMR (128 MHz, Chloroform-*d*, 298 K, relative to $BF_3{\cdot}Et_2O$ /ppm) δ 0.00. FT-IR (KBr, cm^{-1}): ν 3149.1, 3069.4, 1589.4, 1543.4, 1505.8, 1489.5, 1439.9, 1425.7, 1379.4, 1356.8, 1313.4, 1249.2, 1218.0, 1199.3, 1178.3, 1148.5, 1129.1, 1088.6, 1062.4, 1023.8, 982.5, 916.9, 879.0, 866.8, 847.0, 809.5, 798.3, 775.3, 749.8, 741.0, 688.9, 623.4, 600.3, 572.3, 487.2, 476.1. LRMS, m/z 325.1. HRMS m/z found (calcd for $C_{16}H_{13}O_3{}^{10}BF_2Na^+$): 324.0854 (324.0854).

Synthesis of fluoreneBF$_2$ via cascade reaction

Into a round bottom flask were added 9,9-dimethyl fluorene (345 mg, 1.0 mmol), acetic anhydride (5 mL) and boron trifluoride diethyl etherate (0.8 mL). The reaction mixture was heated to 60 °C and stirred for 5 h. Then the reaction was quenched by adding the reaction mixture drop wise into cold water. The precipitates were washed by water for three times and dried under vacuum. The crude product was purified by column chromatography over silica gel using petroleum ether/dichloromethane (1:1) as eluent to give yellow solids with an isolation yield of 50%. The fluoreneBF$_2$ was further purified by three cycles of recrystallization in spectroscopic grade dichloromethane/hexane. Melting point of fluoreneBF$_2$ was measured by DSC to be 230 °C. Single crystals of fluoreneBF$_2$ were also grown from spectroscopic grade dichloromethane/hexane (CCDC 2049504). The synthetic procedures are the same as our previous study (*Adv. Opt. Mater.***2021**, 2100353).

Synthesis of DPFBF$_2$ via cascade reaction

Into a round bottom flask were added 9,9-diphenylfluorene (318.4 mg, 1.0 mmol), acetic anhydride (2 mL) and boron trifluoride diethyl etherate (0.52 mL). The reaction mixture was heated to 60 °C and stirred for 4 h. Then the reaction was quenched by adding the reaction mixture drop wise into cold water. The precipitates were washed by water for three times and dried under vacuum. The crude product was purified by column chromatography over silica gel using petroleum ether/dichloromethane (1:1) as eluent to give yellow solids with an isolation yield of 48%. The DPFBF$_2$ was further purified by three cycles of recrystallization in spectroscopic grade dichloromethane/hexane. ^{1}H NMR (400 MHz, DMSO-*d*$_6$, relative to Me$_4$Si /ppm) δ 8.28 (d, *J* = 8.3 Hz, 1H), 8.23 (d, *J* = 8.2 Hz, 1H), 8.20 (s, 1H), 8.13 (d, *J* = 7.3 Hz, 1H), 7.54-7.44 (m, 3H), 7.36 (s, 1H), 7.33 – 7.25 (m, 6H), 7.16 (d, *J* = 6.7 Hz, 4H), 2.44 (s, 3H). ^{13}C NMR (100 MHz, Chloroform-*d*) δ 191.49, 182.45, 152.87, 152.30, 147.89, 144.57, 138.14, 130.27, 130.05, 129.29, 128.58, 128.05, 128.00, 127.20, 126.70, 126.56, 121.64, 120.75, 97.39, 65.65, 24.68.^{19}F NMR (376 MHz, Chloroform-*d*, 298 K, relative to CFCl$_3$ /ppm) δ -139.00 (20%), -139.07 (80%). ^{11}B

NMR (128 MHz, Chloroform-*d*, 298 K, relative to $BF_3{\cdot}Et_2O$ /ppm) δ 0.01. FT-IR (KBr, cm^{-1}): ν 3149.1, 3069.4, 1589.4, 1543.4, 1505.8, 1489.5, 1439.9, 1425.7, 1379.4, 1356.8, 1313.4, 1249.2, 1218.0, 1199.3, 1178.3, 1148.5, 1129.1, 1088.6, 1062.4, 1023.8, 982.5, 916.9, 879.0, 866.8, 847.0, 809.5, 798.3, 775.3, 749.8, 741.0, 688.9, 623.4, 600.3, 572.3, 487.2, 476.1. HRMS m/z found (calcd for $C_{29}H_{21}O_2BF_2NH_4^+$): 486.1978 (486.1977).

Synthesis of SpiroBF$_2$ via cascade reaction

Into a round bottom flask were added 9,9′-spirobifluorene (500 mg, 1.1 mmol), acetic anhydride (5 mL) and boron trifluoride diethyl etherate (0.8 mL). The reaction mixture was heated to 60 °C and stirred for 5 h. Then the reaction was quenched by adding the reaction mixture dropwise into cold water. The precipitates were washed by water for three times and dried under vacuum. The crude product was purified by column chromatography over silica gel using petroleum ether/dichloromethane (1:1) as eluent to give yellow solids with an isolation yield of 53%. The spiroBF$_2$ was further purified by three cycles of recrystallization in spectroscopic grade dichloromethane/hexane. Melting point of spiroBF$_2$ was measured by DSC to be 166 °C. Single crystals of spiroBF$_2$ were also grown from spectroscopic grade dichloromethane/hexane (CCDC 2049502). The synthetic procedures are the same as our previous study (*Adv. Opt. Mater.***2021**, 2100353).

Preparation of afterglow materials by doping BF$_2$bdk into organic matrices

For the preparation of BF$_2$bdk-TPO-0.5% powders, 500 μL BF$_2$bdk in dichloromethane (1.0 mg/mL) and 100 mg triphenylphosphine oxide (TPO) were added into an agate mortar (diameter = 5 cm). After grinding and solvent evaporating, BF$_2$bdk-TPO-0.5% powders that show afterglow properties were obtained. The other afterglow materials in this study at different doping concentrations, using different BF$_2$bdk luminogens and different organic matrices were prepared through similar processes. TP and TPO possess melting points of 78.5-81.5 °C and 154-158 °C, respectively. The BF$_2$bdk-matrix powders samples were used to prepare the melt-cast

samples. It is found that the molten matrices can dissolve BF_2bdk because of the low doping concentrate ions of BF_2bdk. The melt-cast samples were obtained by heating the powder samples into melt followed by room temperature cooling.

Physical measurements and instrumentation

Nuclear magnetic resonance (NMR) spectra were recorded on a JEOL Fourier-transform NMR spectrometer (400 MHz), including ^{1}H NMR, ^{13}C{^{1}H} NMR, ^{19}F{^{1}H} NMR, ^{11}B{^{1}H} NMR. Mass spectra were performed on Agilent Technologies 5973N and Thermo Fisher Scientific LTQ FT Ultras mass spectrometer. FT-IR spectra were recorded on a Nicolet AVATAR-360 FT-IR spectrophotometer with a resolution of 4 cm^{-1}. Single-crystal X-ray diffraction analysis was performed on a D8 VENTURE SC-XRD instrument. UV-Vis absorption spectra were recorded on a Techcomp UV1050. UV-vis spectrophotometer. The steady-state and delayed emission spectra were collected by Hitachi FL-4700 fluorescence spectrometer equipped with chopping systems; the delayed emission spectra were obtained with a delay time of approximately 1 ms. The excited state decay profiles in millisecond to second region were collected by Hitachi FL-4700 fluorescence spectrometer equipped with chopping systems. The fluorescence decay profiles in nanosecond region were recorded by using time-correlated single photon counting technique (TCSPC) on a Edinburgh FLS1000 fluorescence spectrometer equipped with a picosecond pulsed diode laser. Photoluminescence quantum yield was measured by a Hamamatsu absolute PL quantum yield measurement system based on a standard protocol (*Adv. Mater.* **1997**, *9*, 230). Photographs and videos were captured by HUAWEI P30 cameras. Before the capture, samples were irradiated by a 365 nm UV lamp (5 W) for approximately 5 s at a distance of approximately 15 cm.

TD-DFT calculations

TD-DFT calculations were performed on ORCA 4.2.1 program with B3LYP functional and def2-TZVP(-f) basis set to study the photophysical properties of

molecularly dispersed BF_2bdk in the solid state. Since the afterglow properties are originated from the excited states of molecularly dispersed BF_2bdk in the rigid TPO matrices where intermolecular rotation and vibration are largely restricted, the optimized geometry of BF_2bdk ground state was used for all the TD-DFT calculations. The optimized geometry of BF_2bdk ground state was obtained by a DFT calculation from its single crystal structure using B3LYP functional and def2-TZVP (-f) basis set. Spin-orbit coupling (SOC) matrix elements between the singlet excited states and triplet excited states were calculated with spin-orbit mean-field (SOMF) methods. The obtained electronic structures were analyzed by Multiwfn software. All isosurface maps to show the electron distribution and electronic transitions were rendered by Visual Molecular Dynamics (VMD) software based on the exported files from Multiwfn. (F. Neese, *Wiley Interdiscip. Rev.: Comput. Mol. Sci.* **2018**, *8*, 1327-1332; A. D. Becke, *Phys. Rev. A* **1988**, *38*, 3098-3100; C. Lee, W. Yang, R. G. Parr, *Phys. Rev. B* **1988**, *37*, 785-789; B. Miehlich, A. Savin, H. Stoll, H. Preuss, *Chem. Phys. Lett.* **1989**, *157*, 200-206; F. Weigend, R. Ahlrichs, *Phys. Chem. Chem. Phys.* **2005**, *7*, 3297-3305; T. Lu, F. Chen, *J. Comput. Chem.* **2012**, *33*, 580-592; W. Humphrey, A. Dalke, K. Schulten, *J. Mol. Graphics* **1996**, *14*, 33-38).

Text S1. About BF_2bdk aggregation in organic matrices.

Table S2 summarizes the fluorescence maxima and phosphorescence maxima of the emission spectra of BF_2bdk-TPO-0.01% (Fig. 5A) and BF_2bdk-TPO-0.5% (Fig. 2A) samples. It is found that the emission maxima in the steady-state emission spectra

showed red-shifted behaviors when increasing the doping concentration from 0.01% to 0.5%. These suggest the molecular aggregation of BF_2bdk in organic matrices at 0.5% doping concentrations; at 0.01% doping concentration, the BF_2bdk compounds should be molecularly dispersed in the matrices. In the case of DPFBF_2-TPO, the DPFBF_2-TPO-0.5% powders (λ_F, 463 nm) showed significant red shift in the steady-state emission spectra when compared to the DPFBF_2-TPO-0.01% powders (λ_F, 440 nm). Besides, the ratio of delayed fluorescence band/phosphorescence band of DPFBF_2-TPO-0.5% powders is smaller than that of DPFBF_2-TPO-0.01% powders. These can be explained as: BF_2bdk aggregates cause red shift of steady-state emission spectra but have a less contribution to delayed fluorescence than monomeric dopants, which agree with our previous studies (*Angew. Chem. Int. Ed.* **2021**, *60*, 17138; *Chem. Eng. J.* **2022**, *431*, 134197).

Text S2. Dipole-dipole interactions for the population of triplet excited states.

Because of the dipole-dipole interaction between BF_2bdk's S_1 states and TPO matrices, both ISC and RISC can be enhanced in BF_2bdk-TPO systems, and TADF afterglow has also been switched on. For the population of triplet states in organic systems with the involvement of TADF (*Adv. Mater.* **2014**, *26*, 7931), it can be expressed as $d[T_1]/dt = k_{ISC}[S_1] - (k_{RISC} + k_P + k_{nr})[T_1]$. In most organic systems (including the BF_2bdk-matrix system in the present study), $[S_1]$ should be much larger than or on the same order of magnitude to $[T_1]$. Meanwhile, k_{ISC} is much larger than k_{RISC}. Because of these, the equation shows that the increase of k_{ISC} would lead to

relatively large increase of T_1 population, while the increase of k_{RISC} only leads to relatively small decrease of T_1 population. Overall, the dipole-dipole interaction between BF_2bdk's S_1 states and TPO matrices leads to the increase of T_1 population and consequently the emergence of organic afterglow in the present study when TP is oxidized into TPO.

Text S3. TP matrices can also provide rigid microenvironments to inhibit nonradiative deactivation of dopants' triplets and protect dopants' triplets from oxygen quenching in the reported studies (*Angew. Chem. Int. Ed*. **2020**, *59*, 16054). We didn't emphasize this because the BF_2bdk-TP samples showed insignificant organic afterglow. The absence of organic afterglow of BF_2bdk-TP samples is caused by the lack of dipole-dipole interactions between BF_2bdk and TP and consequently inefficient intersystem crossing of BF_2bdk.

Text S4. The comparison between TD-DFT results and experimental results

Table S3 summarizes the energy levels of S_1 and T_1 for the comparison between TD-DFT results and experimental results. In this study, TD-DFT calculations were performed on ORCA 4.2.1 program with B3LYP functional and def2-TZVP(-f) basis set. The optimized geometry of BF_2bdk's ground state was used for TD-DFT calculations. In this study (in the case of fluoreneBF_2 and spiroBF_2) and our previous studies on BF_2bdk-matrix systems (*ACS Appl. Mater. Interfaces* **2022**, *14*, 1587), it has been found that BF_2bdk's T_1 energy levels calculated by TD-DFT are close to

those estimated from their phosphorescence maxima. Because of this, we use phosphorescence maxima to estimate BF_2bdk's T_1 energy levels in the present study. For BF_2bdk's S_1 energy levels, it has been found that the S_1 energy levels calculated by TD-DFT match the experimental UV-vis absorption maxima in this study (for example, in the case of fluoreneBF_2 and DPFBF_2) and also in our previous studies (*Angew. Chem. Int. Ed.* **2021**, *60*, 17138; *Adv. Funct. Mater.* **2021**, 2110207). So we use these S_1 energy levels and their electron-hole isosurface maps, as well as the UV-vis absorption spectra, to study the absorption properties of BF_2bdk solutions. It is noted that, because of the Stokes shift, the S_1 energy levels estimated from the fluorescence maxima are significantly lower than those calculated by TD-DFT using BF_2bdk's ground state geometry.

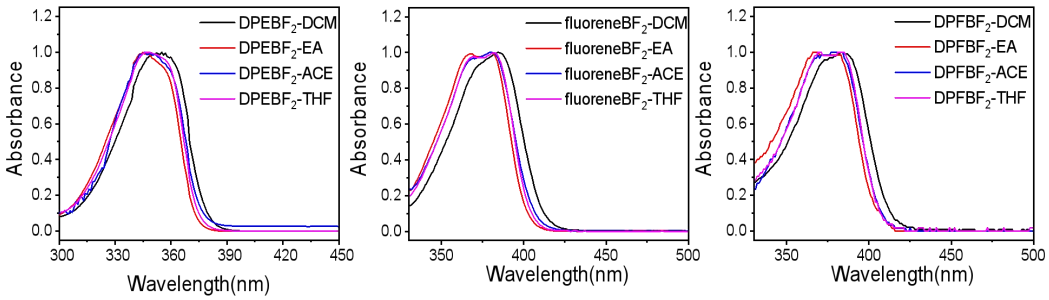

Fig. S1. UV-vis spectra of BF_2bdk in different solvents. DCM, EA, ACE and THF refer to dichloromethane, ethyl acetate, acetone and tetrahydrofuran, respectively. In the case of DPEBF_2, fluoreneBF_2 and DPFBF_2, the electron-hole isosurface map of the S_1 states (by TD-DFT calculations, vide infra) showed intramolecular charge transfer plus localized excitation characters. Their UV-vis absorption spectra showed intense absorption bands with some structures, which also suggest the intramolecular charge transfer plus localized excitation characters in DPEBF_2, fluoreneBF_2 and DPFBF_2 systems.

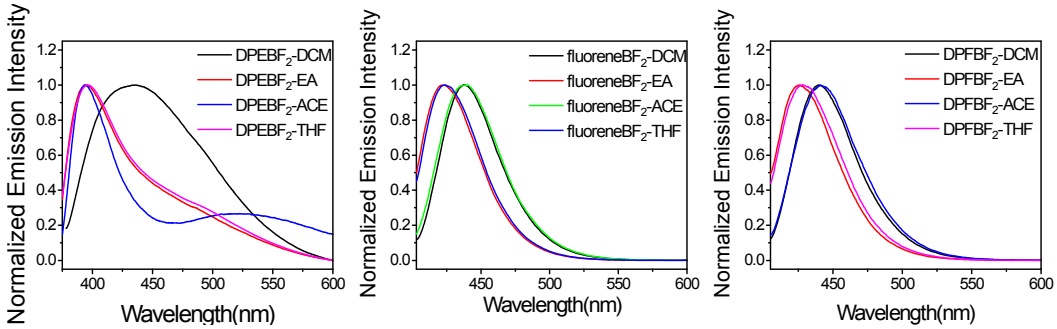

Fig. S2. Room-temperature steady-state emission spectra of BF_2bdk in different solvents. DCM, EA, ACE and THF refer to dichloromethane, ethyl acetate, acetone and tetrahydrofuran, respectively. For the emission spectra of $DPEBF_2$ solutions, we have repeated the measurements. It turns out that the emission spectra of $DPEBF_2$ in dichloromethane are broad. $DPEBF_2$ possess ICT characters. The free-rotating single bonds of O-C-O functional group and C-C bonds between boron(III) diketonate and aromatic moiety allow $DPEBF_2$ molecule to adopt diverse conformation. These motivate us to propose that $DPEBF_2$ in dichloromethane shows twisted intramolecular charge transfer (TICT) emission characters (*J. Phys. Chem. C* **2016**, *120*, 22539).

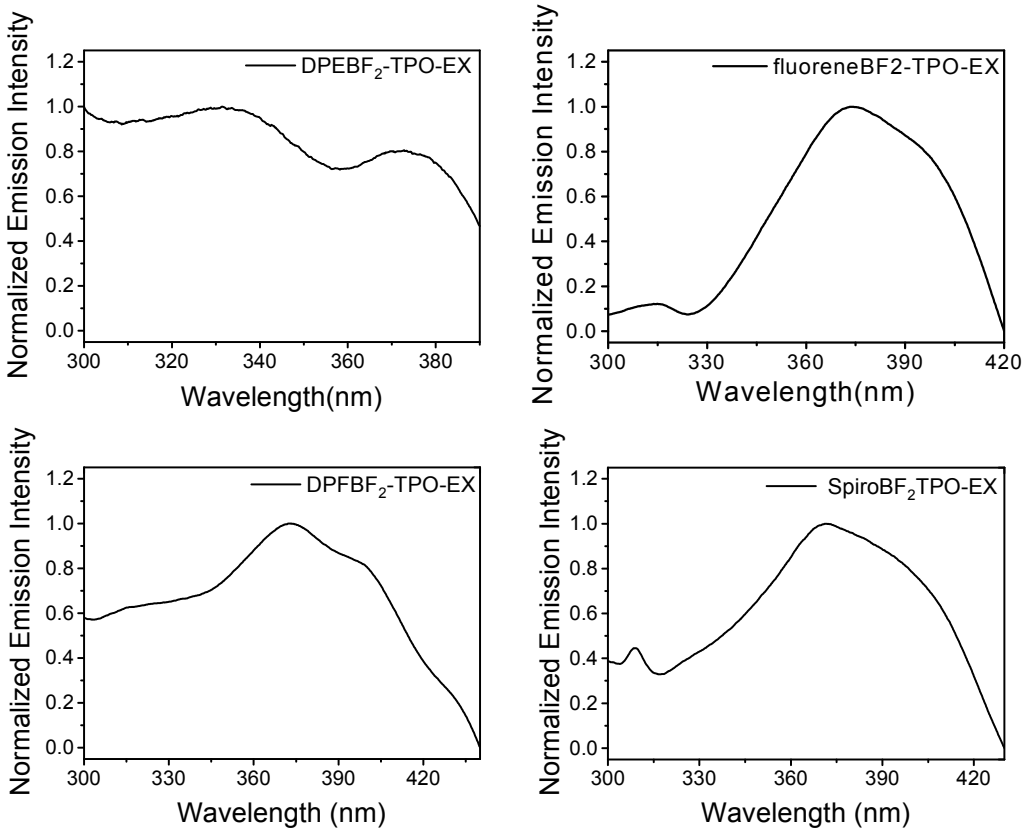

Fig. S3. Excitation spectra of BF_2bdk-TPO samples.

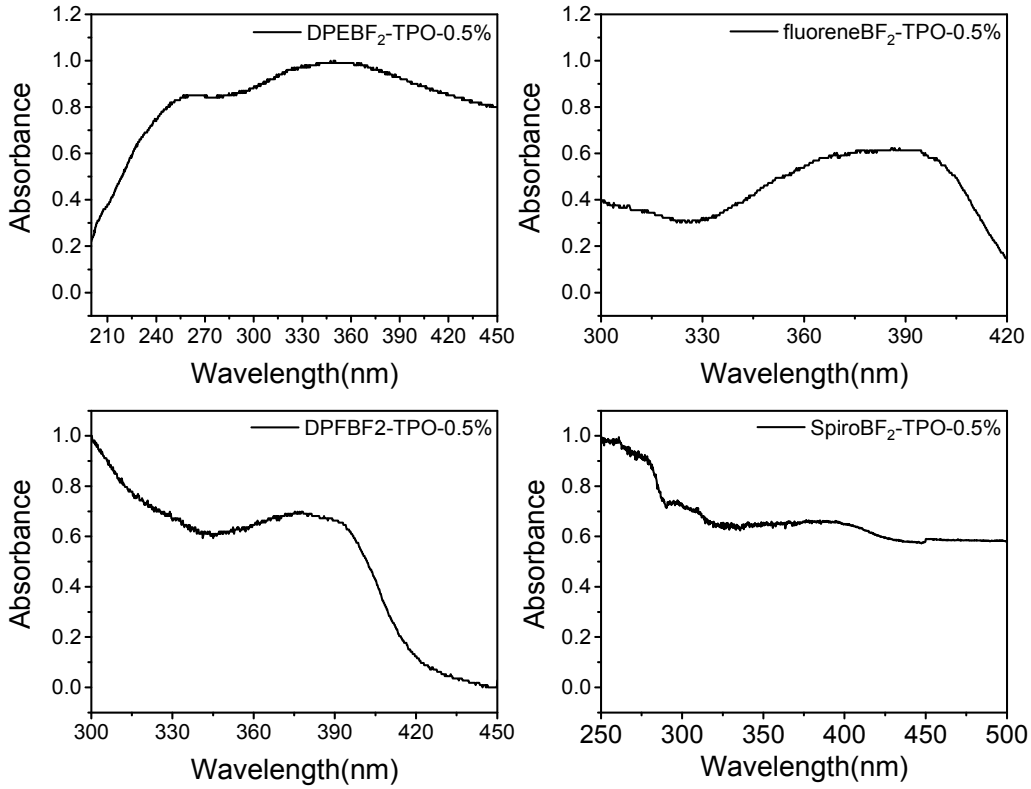

Fig. S4. UV-vis spectra of BF_2bdk-TPO-0.5% samples.

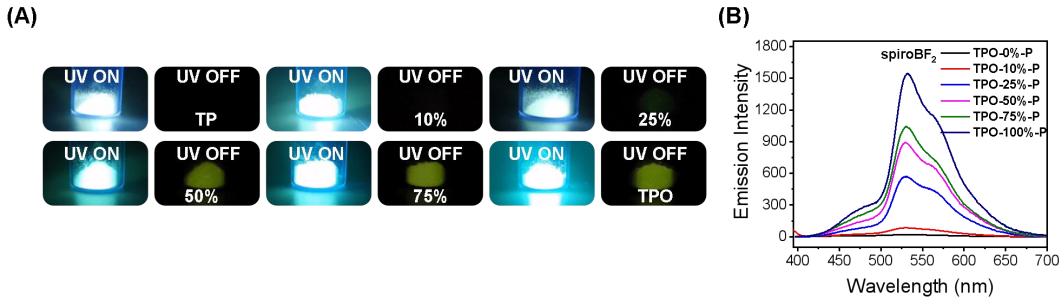

Fig. S5. (A) Photographs of the spiroBF_2-TP-TPO powders with different TPO contents. (B) Delayed emission (1 ms delay) spectra of spiroBF_2-TP-TPO samples with different TPO contents. TP plus TPO matrices with different TPO contents (0%, 10%, 25%, 50%, 75% and 100%) have been used to accommodate BF_2bdk. It is found that when the TPO contents increase to 25%, the spiroBF_2-TP-TPO powders exhibited room-temperature afterglow which can be observed by human eyes in a dark room.

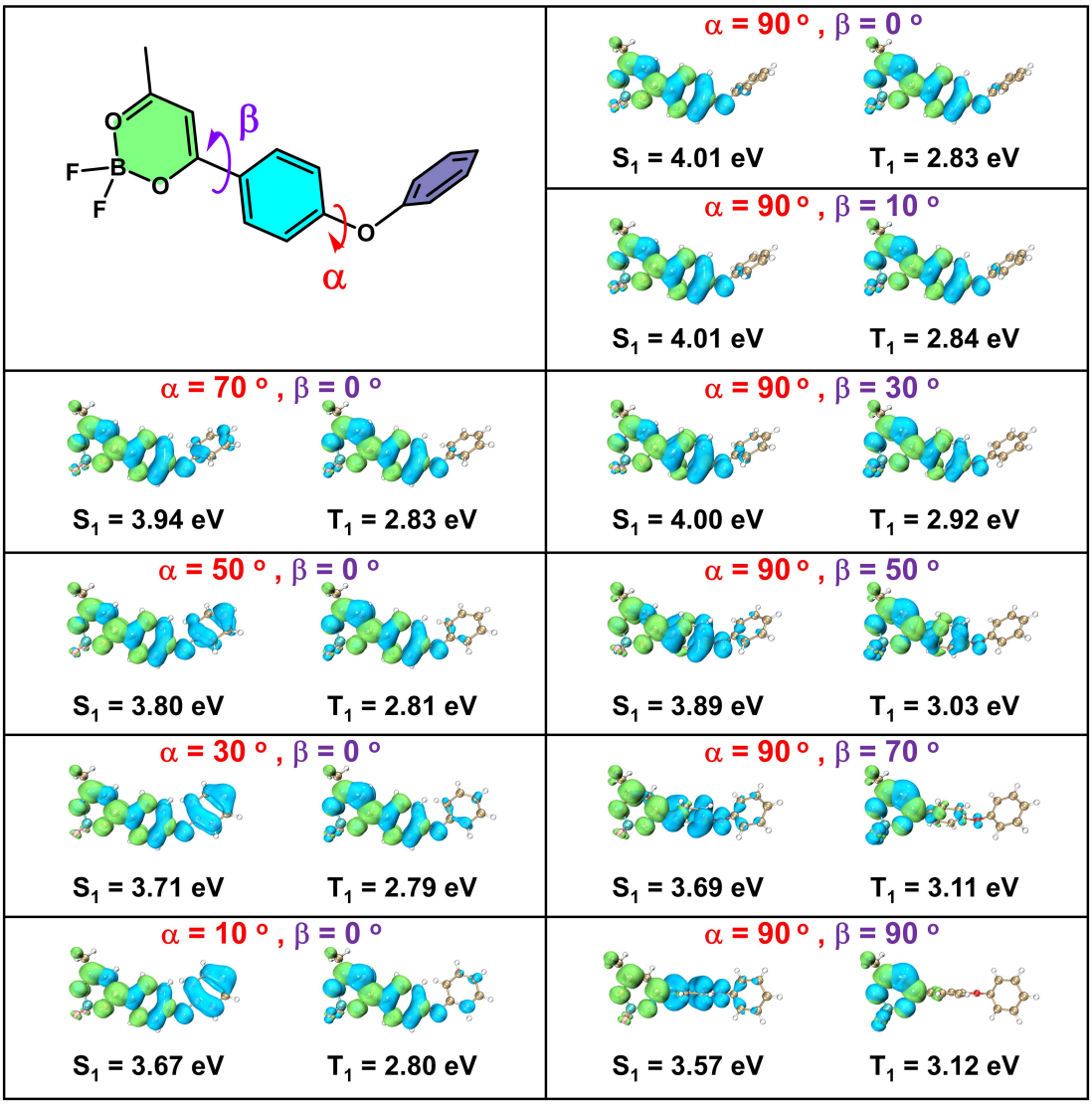

Fig. S6. S_1 and T_1 levels of $DPEBF_2$ with different conformation obtained by TD-DFT calculation. The conformation is defined by the twisted angles (that is, the dihedral angles) α and β. In the main text, the fluorescence maxima of $DPEBF_2$ showed insignificant change in TPO and TP (Fig. 5); it is proposed that twist-induced spectral shifts offset the effect of dipole-dipole interactions. Dipole-dipole interactions between TPO and $DPEBF_2$'s S_1 state lead to red-shifted fluorescence. By TD-DFT calculations, it is found that the increase of twist angle α leads to the increase of S_1 levels and insignificant change of T_1 levels, while the increase of twist angle β leads to the decrease of S_1 levels and increase of T_1 levels. Since the phosphorescence maxima in the delayed emission spectra of $DPEBF_2$-TPO-0.01% powders were similar to those of $DPEBF_2$-TP-0.01% powders (Fig. 5). We propose that $DPEBF_2$ in TPO matrices possesses a larger twist angle α, that is, a more twisted conformation

than in TP matrices; the twisted conformation lead to blue-shifted fluorescence. Therefore, in the case of $DPEBF_2$, the twist-induced spectral shifts offset the effect of dipole-dipole interactions. It is noted that, although the S_1 and T_1 levels by TD-DFT calculations may be different from those estimated from emission spectra, the trend of S_1 and T_1 levels by systematically varying the twisted angles can still be used to interpret the spectral observations in $DPEBF_2$-TPO and $DPEBF_2$-TP samples. We think it is understandable that this trend of S_1 and T_1 levels can still support our statement "it is proposed that twist-induced spectral shifts offset the effect of dipole-dipole interactions" in the main text.

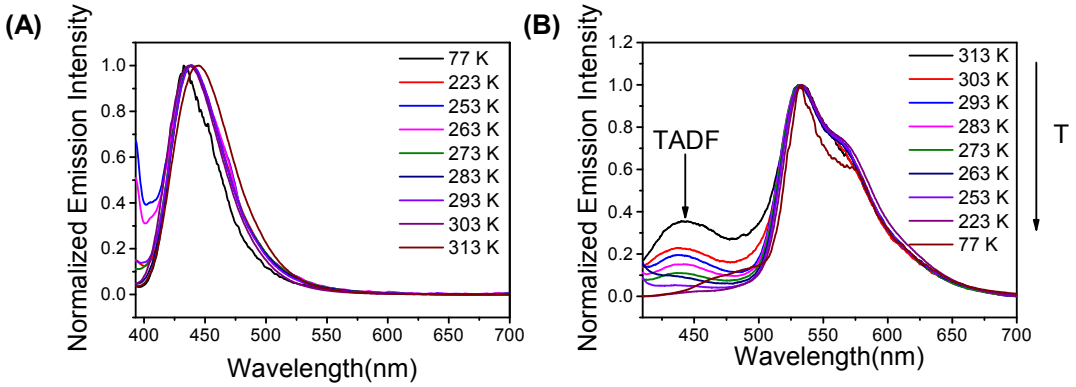

Fig. S7. (A) Variable-temperature steady-state and (B) delayed emission (1 ms delay) spectra of $DPFBF_2$-TPO-0.01% powders.

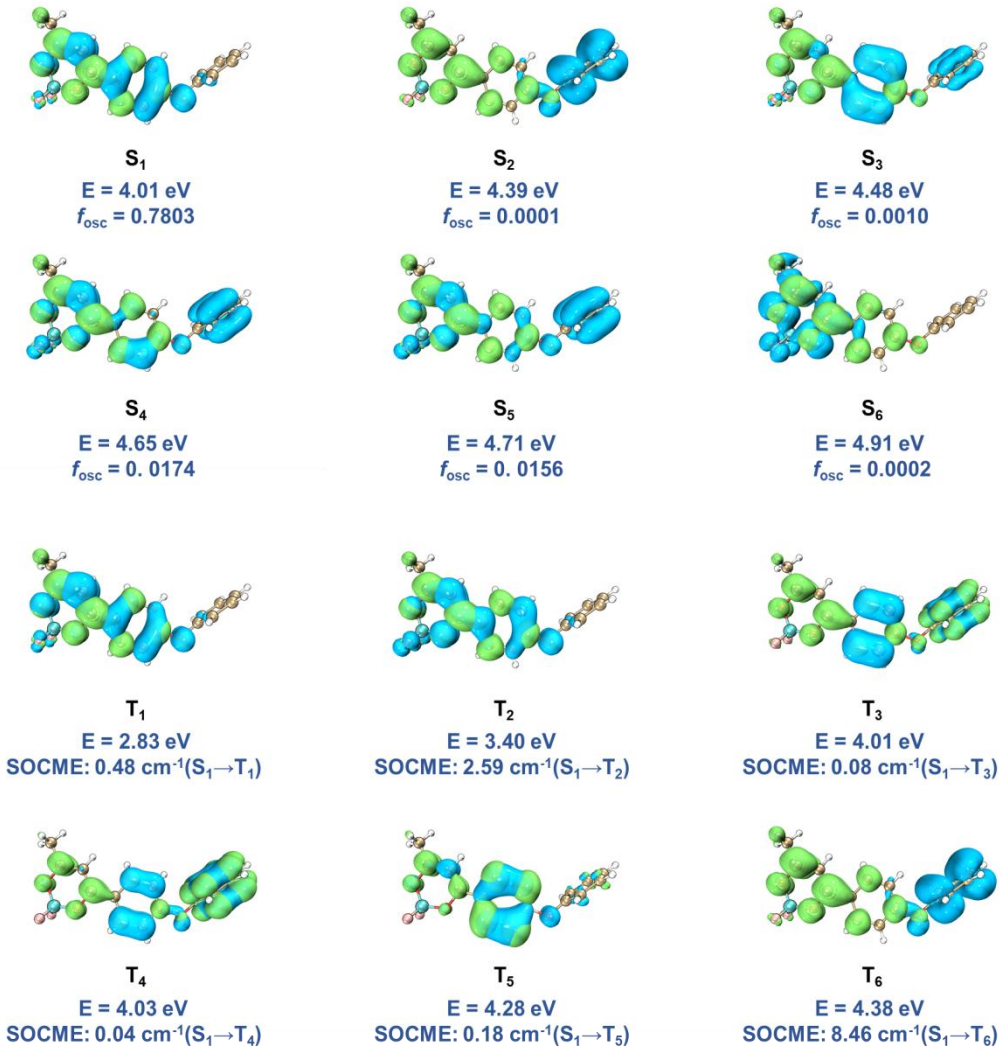

Fig. S8. The TD-DFT calculated results of $DPEBF_2$ singlet and triplet excited states. The ΔE_{ST} value is estimated from fluorescence and phosphorescence maxima in Fig. 5 to be 0.46 eV. The energy level of T_2 state is sandwiched between S_1 and T_1. Therefore, the S_1-to-T_6 ISC channel with relatively small singlet-triplet energy gap and relatively large SOCME of 8.46 cm^{-1} can mediate the intersystem crossing of $DPEBF_2$ system.

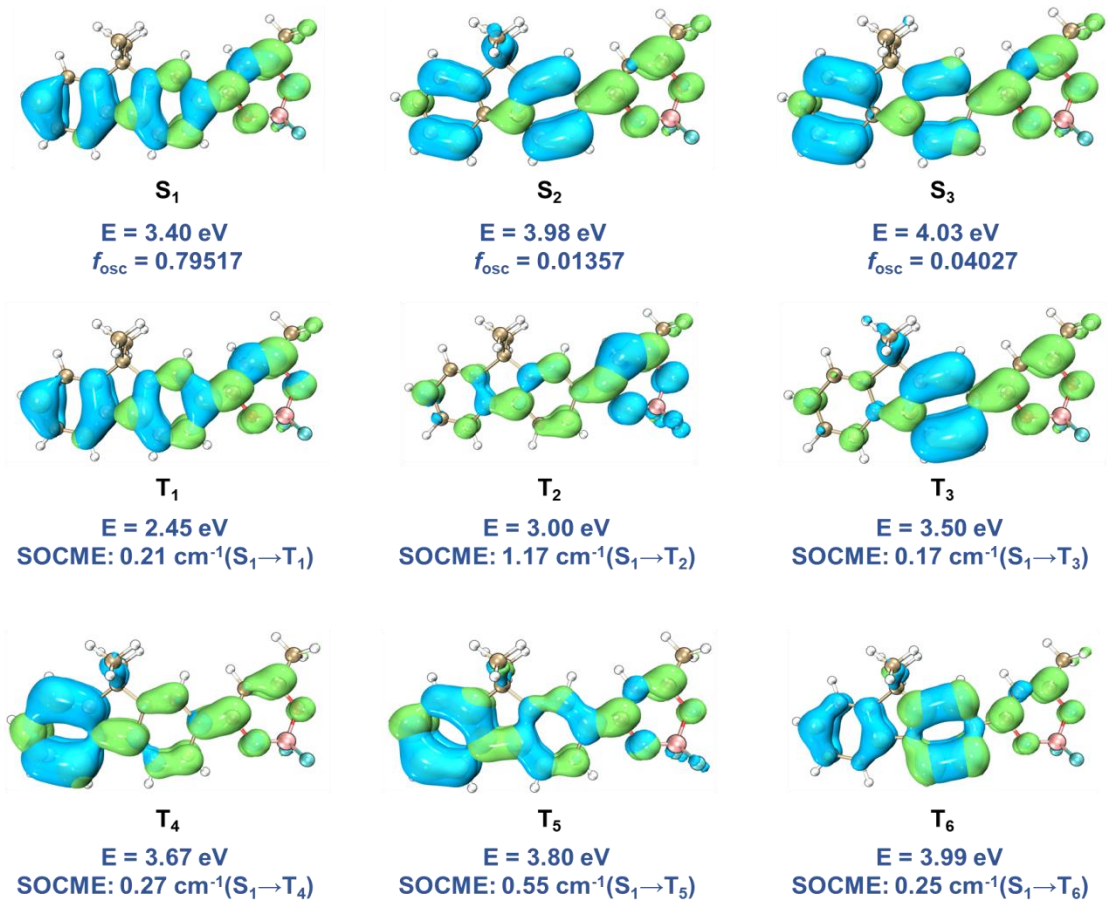

Fig. S9. The TD-DFT calculated results of fluoreneBF$_2$ singlet and triplet excited states. The ΔE_{ST} value is estimated from fluorescence and phosphorescence maxima in Fig. 5 to be 0.52 eV. The energy level of T_2 state should be sandwiched between S_1 and T_1. Therefore, the S_1-to-T_2 ISC channel with relatively small singlet-triplet energy gap and relatively large SOCME of 1.17 cm^{-1} can mediate the intersystem crossing of fluoreneBF$_2$ system.

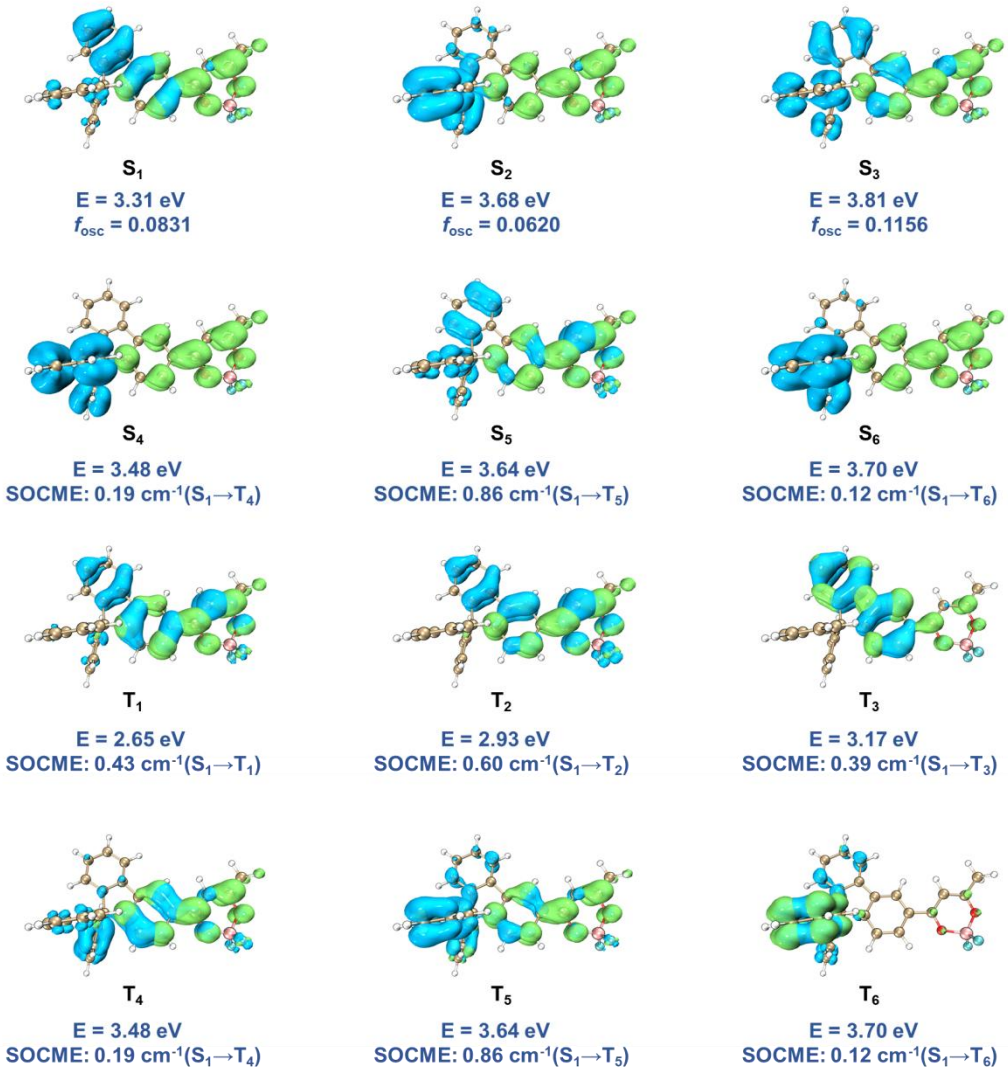

Fig. S10. The TD-DFT calculated results of $DPFBF_2$ singlet and triplet excited states. The TD-DFT calculated results of fluoreneBF_2 singlet and triplet excited states. The ΔE_{ST} value is estimated from fluorescence and phosphorescence maxima in Fig. 5 to be 0.48 eV. The energy level of T_2 state should be sandwiched between S_1 and T_1. Therefore, the S_1-to-T_5 ISC channel with relatively small singlet-triplet energy gap and relatively large SOCME of 0.86 cm^{-1} can mediate the intersystem crossing of $DPFBF_2$ system.

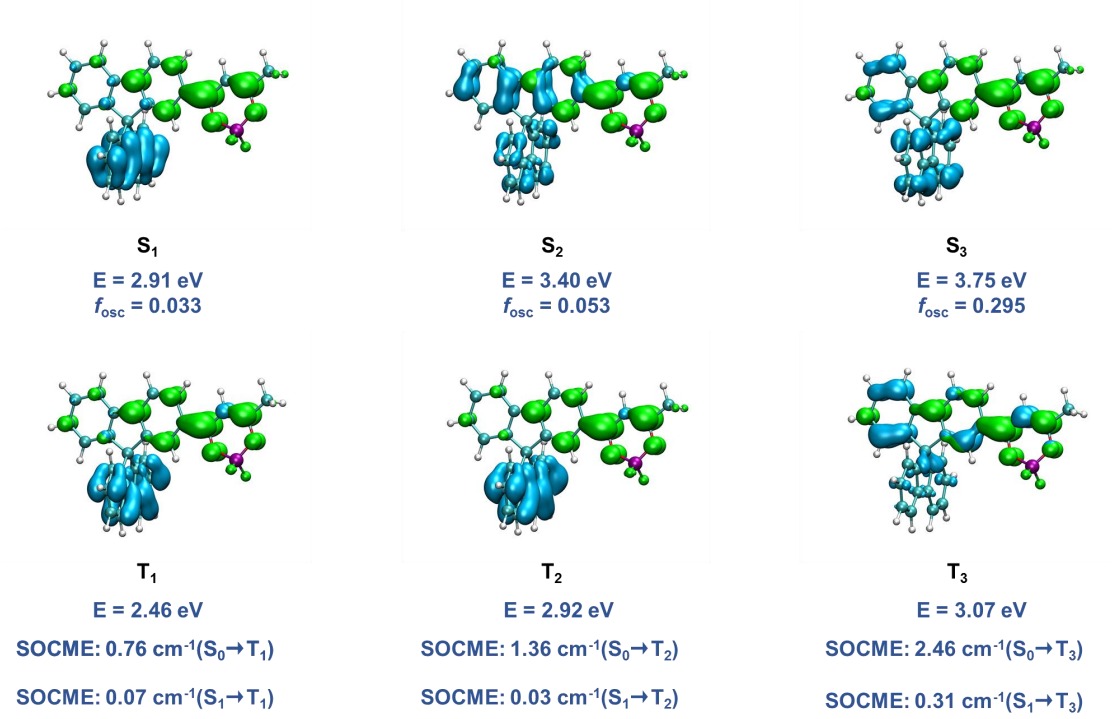

Fig. S11. The TD-DFT calculated results of spiroBF$_2$ singlet and triplet excited states. The S_1-to-T_3 ISC channel with relatively small singlet-triplet energy gap and relatively large SOCME of 0.31 cm^{-1} can mediate the intersystem crossing of spiroBF$_2$ system.

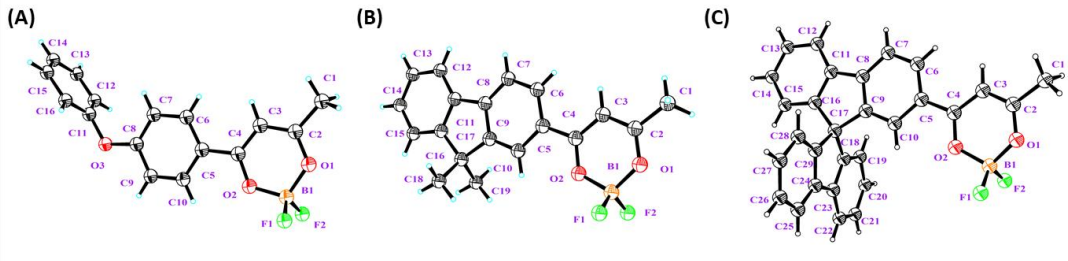

Fig. S12. Single crystal structures of (A) DPEBF$_2$, (B) fluoreneBF$_2$ and (C） spiroBF$_2$.

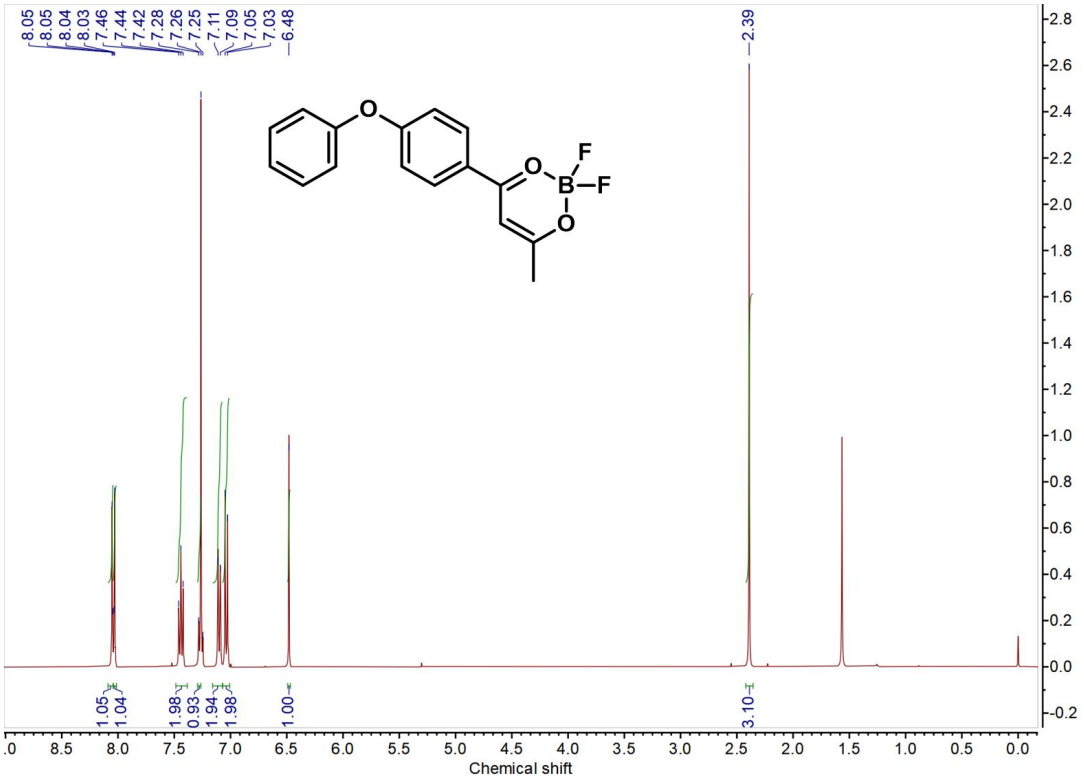

Fig. S13. ^{1}H NMR spectra of $DPEBF_2$.

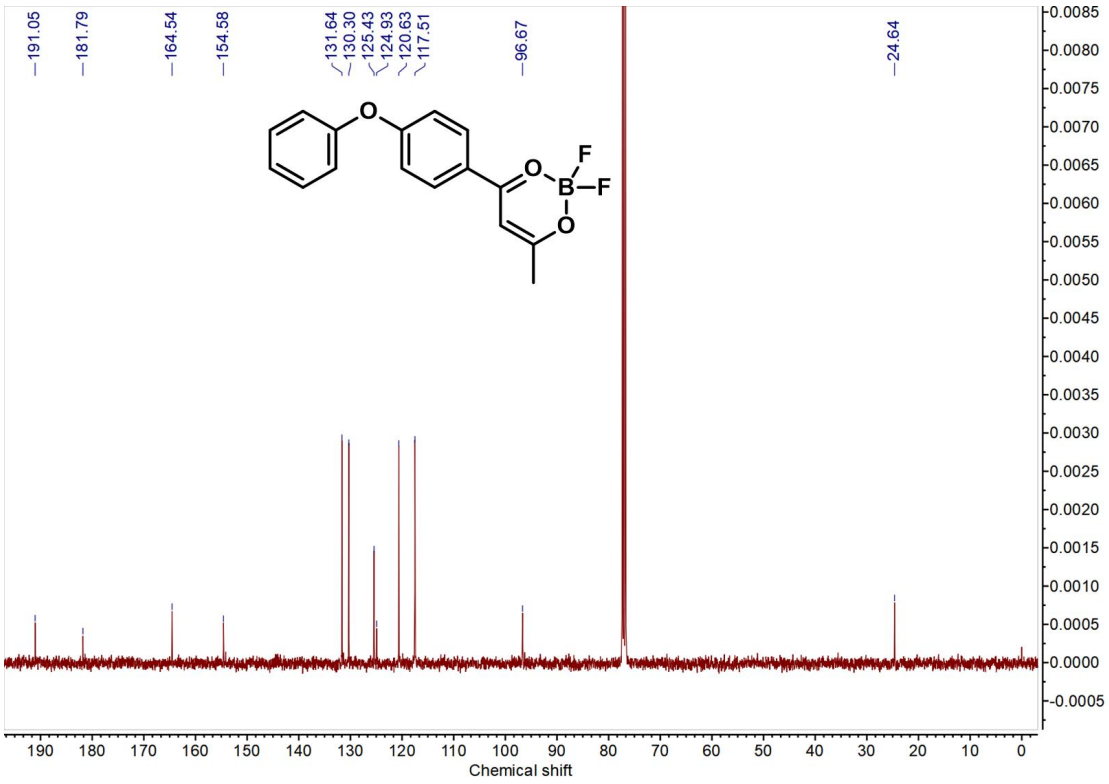

Fig. S14. ^{13}C NMR spectra of $DPEBF_2$.

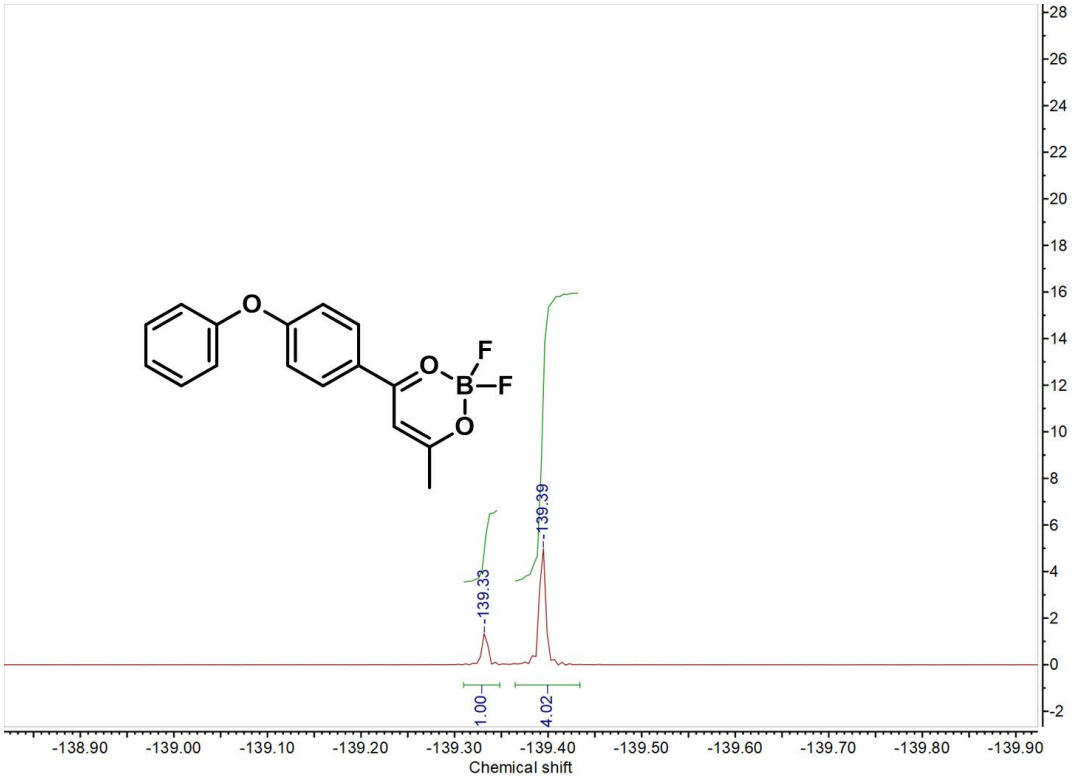

Fig. S15. ^{19}F NMR spectra of $DPEBF_2$.

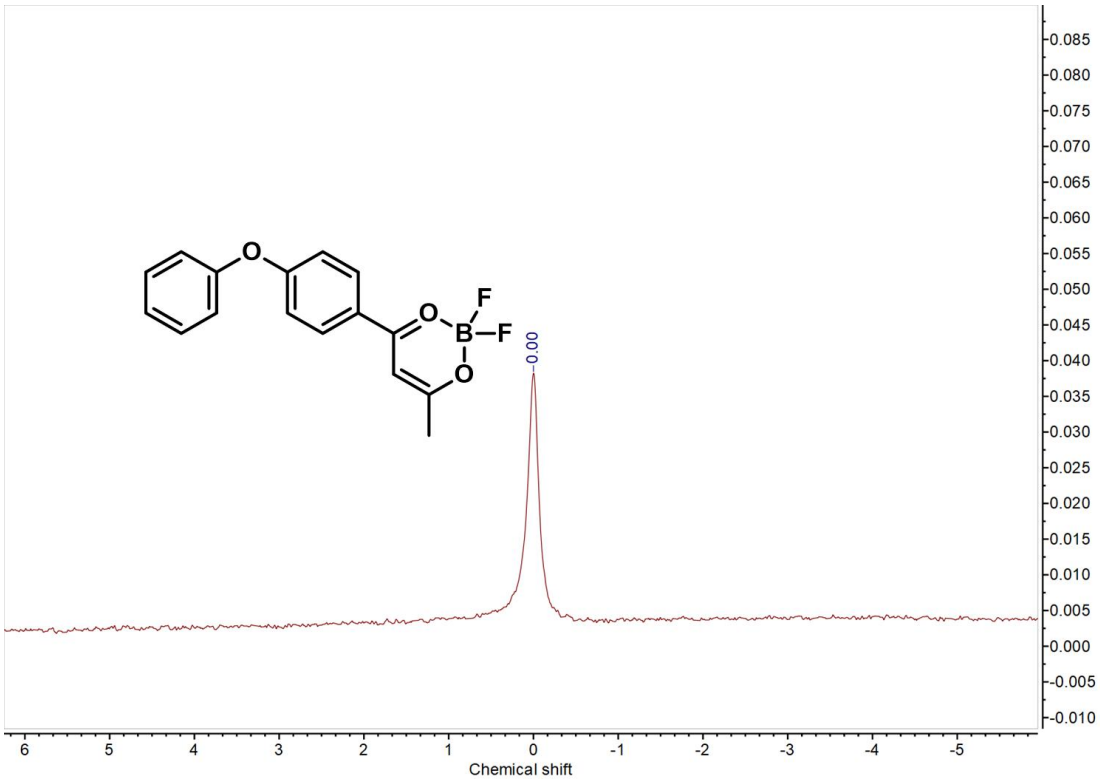

Fig. S16. ^{11}B NMR spectra of $DPEBF_2$.

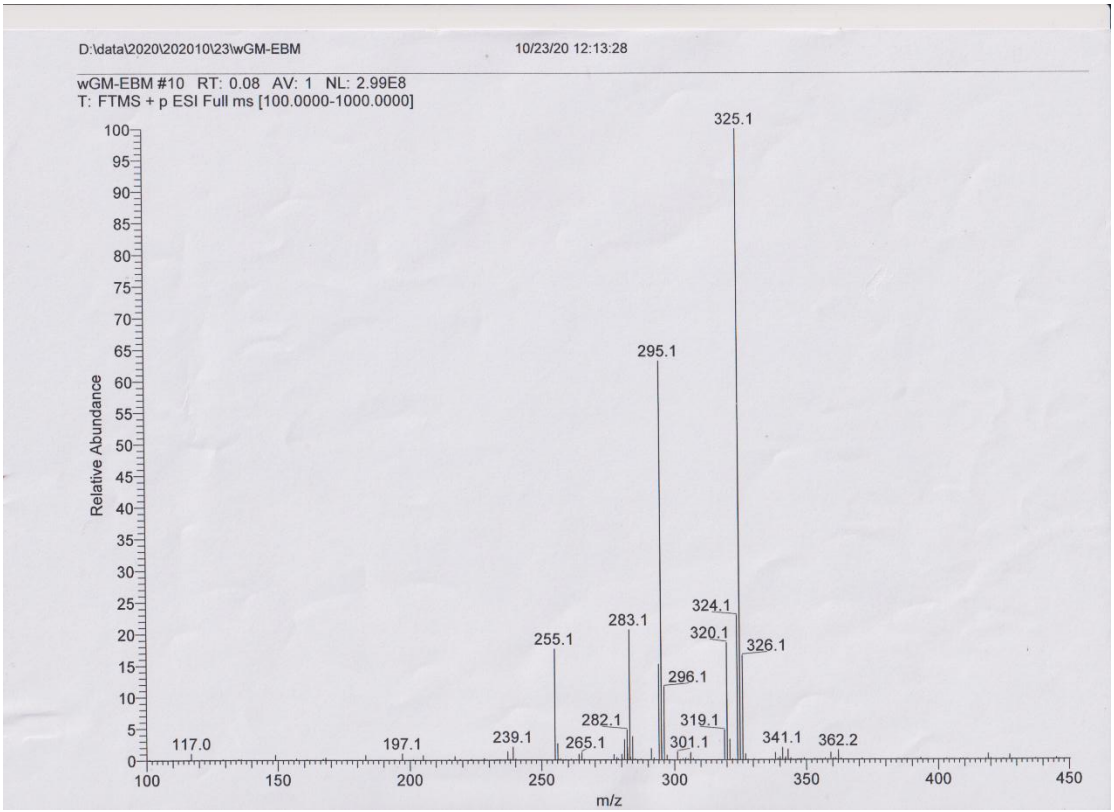

National Center for Organic Mass Spectrometry in Shanghai
Shanghai Institute of Organic Chemistry
Chinese Academic of Sciences
High Resolution ESI-MS REPORT

Instrument: Thermo Scientific Q Exactive HF Orbitrap-FTMS

Card Serial Number: E202066

Sample Serial Number: Wgm-EBM

Operator: Songw Date: 2020/10/26

Operation Mode: ESI Positive Ion Mode

Elemental composition search on mass 324.09

m/z= 319.09-329.09

m/z	Theo. Mass	Delta (ppm)	RDB equiv.	Composition
324.0854	324.0854	0.05	9.5	$C_{16}H_{13}O_3{}^{10}BF_2Na$
	324.0843	3.58	13.5	$C_{19}H_{12}O_2{}^{10}BFNa$
	324.0869	-4.55	14.0	$C_{19}H_{13}O_2N_2Na$

Fig. S17. LRMS and HRMS spectra of $DPEBF_2$.

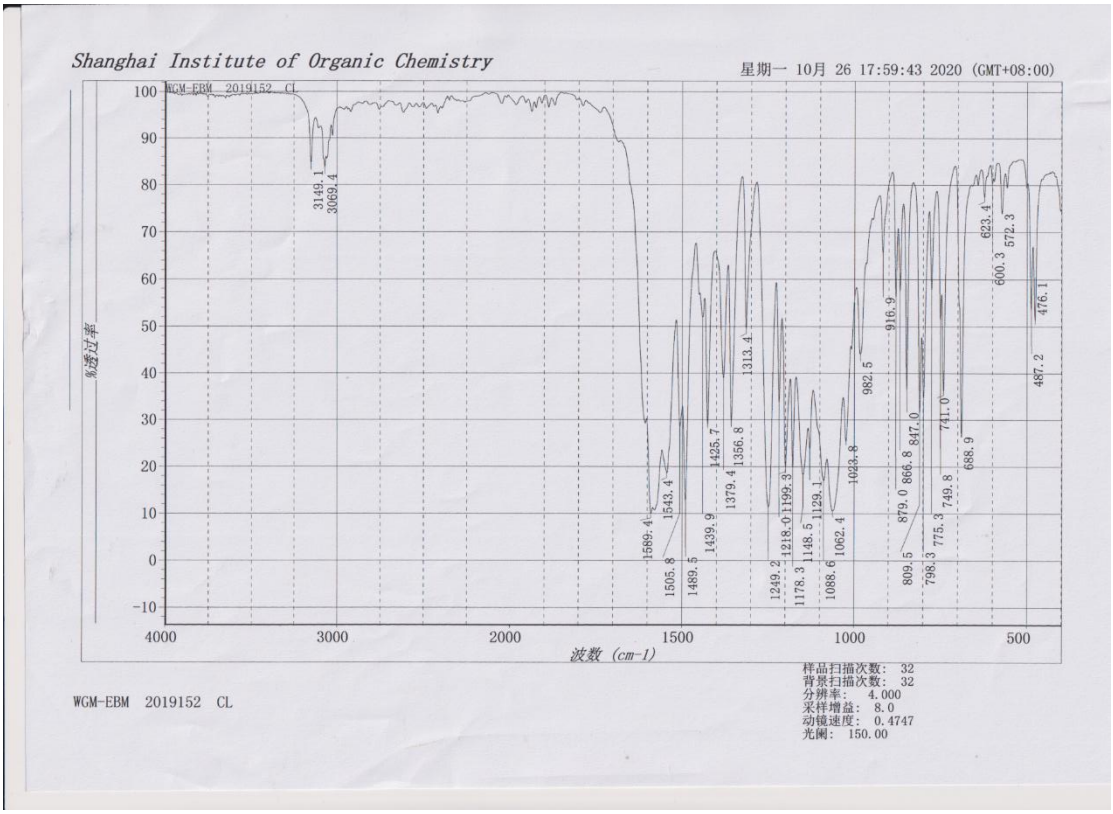

Fig. S18. FT-IR spectra of $DPEBF_2$.

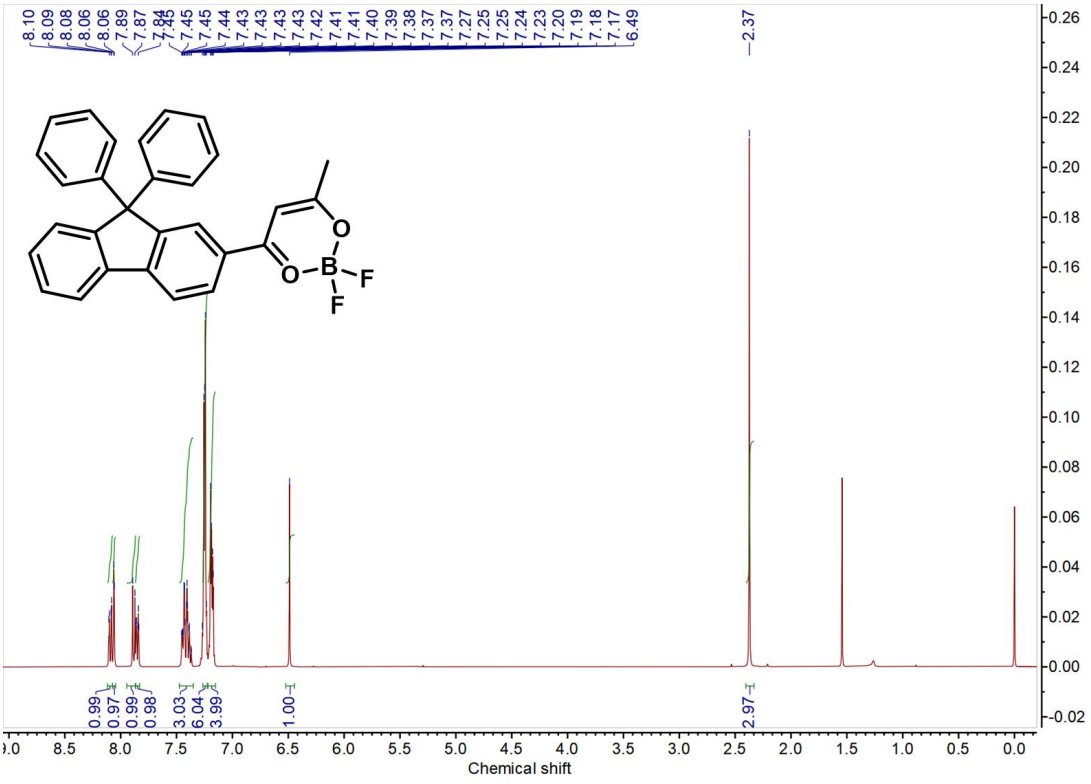

Fig. S19. ^1H NMR spectra of $DPFBF_2$.

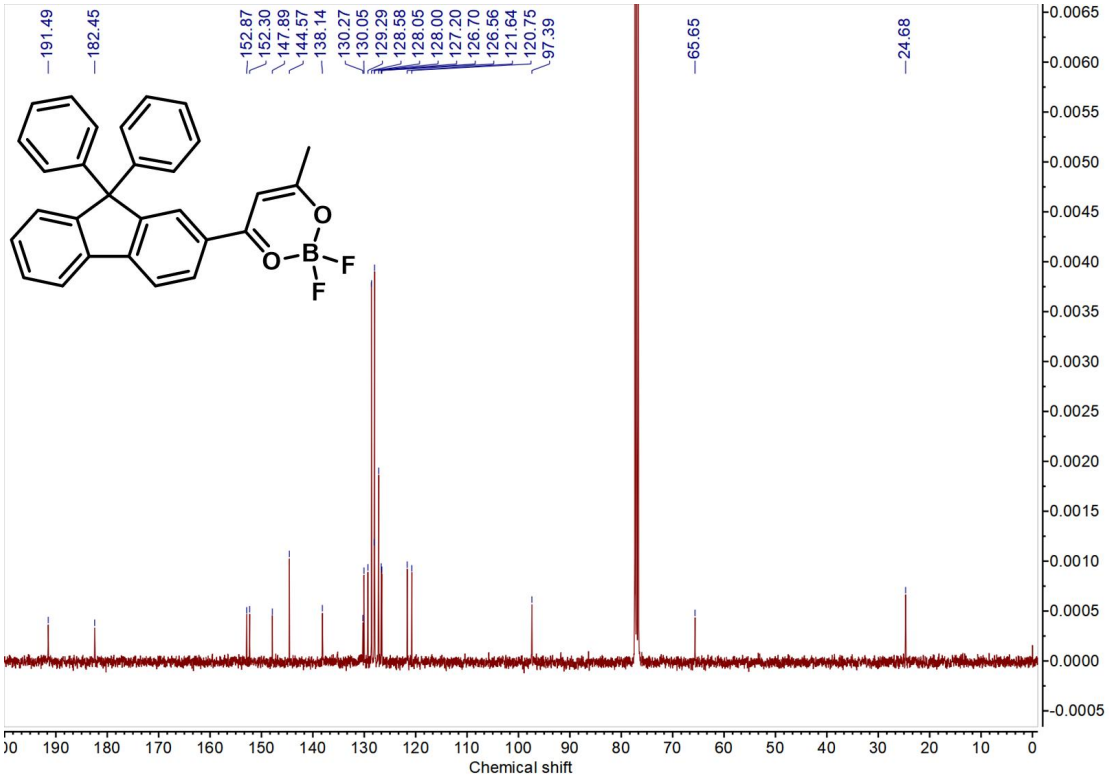

Fig. S20. ^{13}C NMR spectra of $DPFBF_2$.

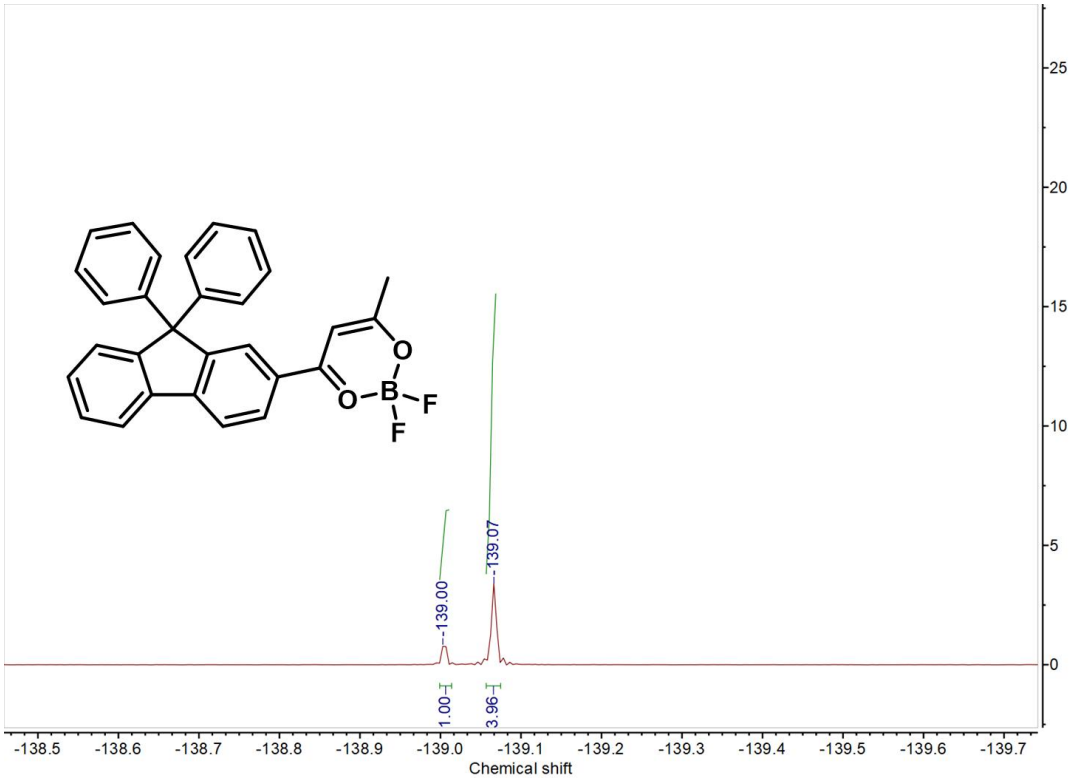

Fig. S21. ^{19}F NMR spectra of $DPFBF_2$.

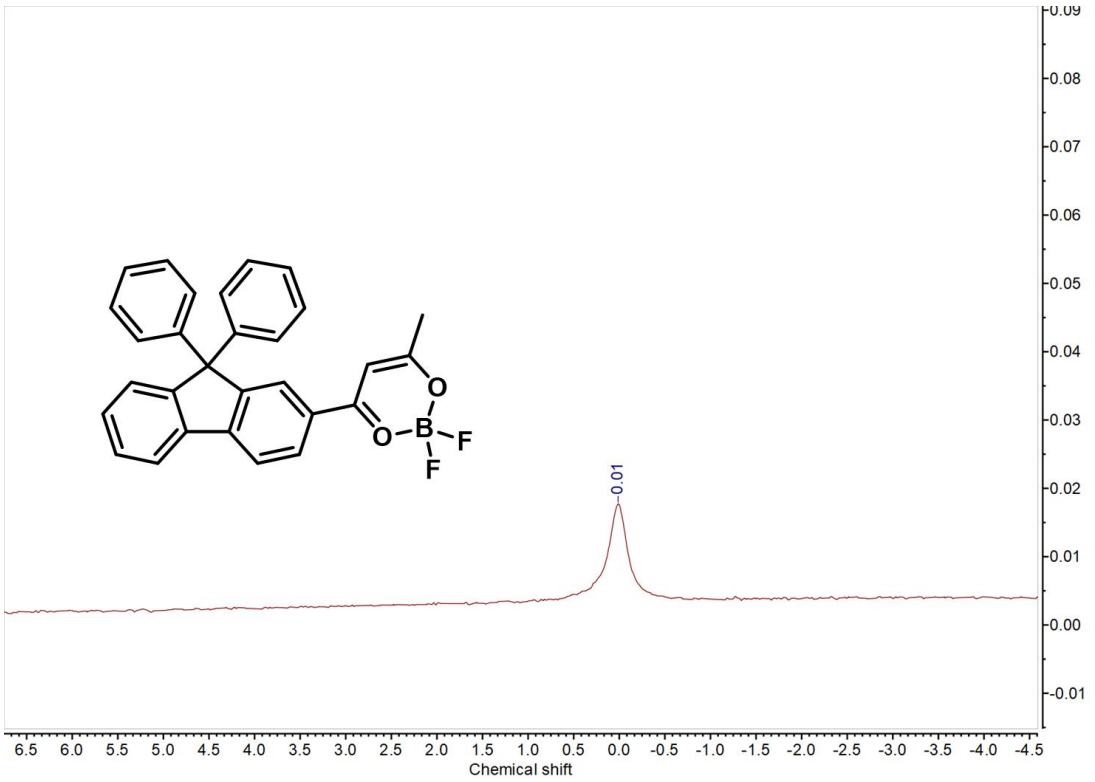

Fig. S22. ^{11}B NMR spectra of $DPFBF_2$.

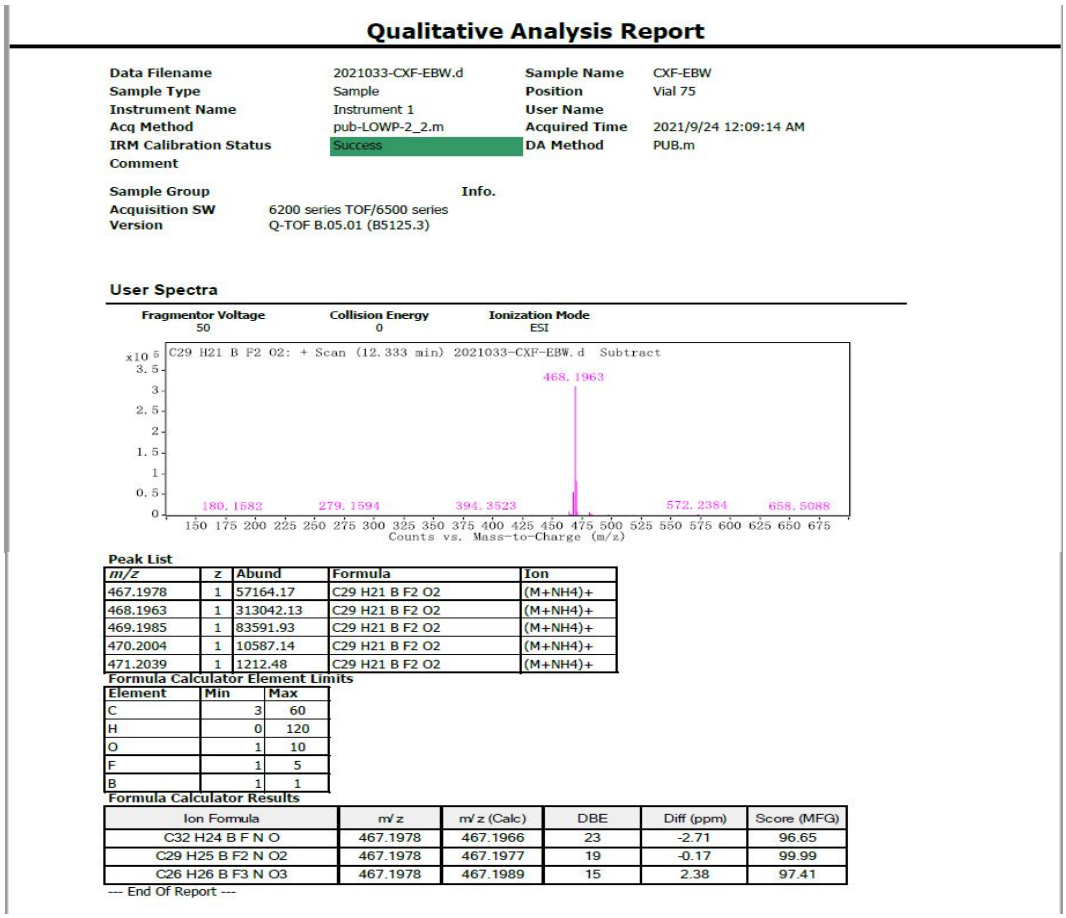

Qualitative Analysis Report

Data Filename	2021033-CXF-EBW.d	**Sample Name**	CXF-EBW
Sample Type	Sample	**Position**	Vial 75
Instrument Name	Instrument 1	**User Name**	
Acq Method	pub-LOWP-2_2.m	**Acquired Time**	2021/9/24 12:09:14 AM
IRM Calibration Status	Success	**DA Method**	PUB.m
Comment			

Sample Group	**Info.**
Acquisition SW Version	6200 series TOF/6500 series Q-TOF B.05.01 (B5125.3)

User Spectra

Fragmentor Voltage	**Collision Energy**	**Ionization Mode**
50	0	ESI

Peak List

m/z	z	Abund	Formula	Ion
467.1978	1	57164.17	C29 H21 B F2 O2	(M+NH4)+
468.1963	1	313042.13	C29 H21 B F2 O2	(M+NH4)+
469.1985	1	83591.93	C29 H21 B F2 O2	(M+NH4)+
470.2004	1	10587.14	C29 H21 B F2 O2	(M+NH4)+
471.2039	1	1212.48	C29 H21 B F2 O2	(M+NH4)+

Formula Calculator Element Limits

Element	Min	Max
C	3	60
H	0	120
O	1	10
F	1	5
B	1	1

Formula Calculator Results

Ion Formula	m/z	m/z (Calc)	DBE	Diff (ppm)	Score (MFG)
C32 H24 B F N O	467.1978	467.1966	23	-2.71	96.65
C29 H25 B F2 N O2	467.1978	467.1977	19	-0.17	99.99
C26 H26 B F3 N O3	467.1978	467.1989	15	2.38	97.41

--- End Of Report ---

Fig. S23. MS spectra of $DPFBF_2$.

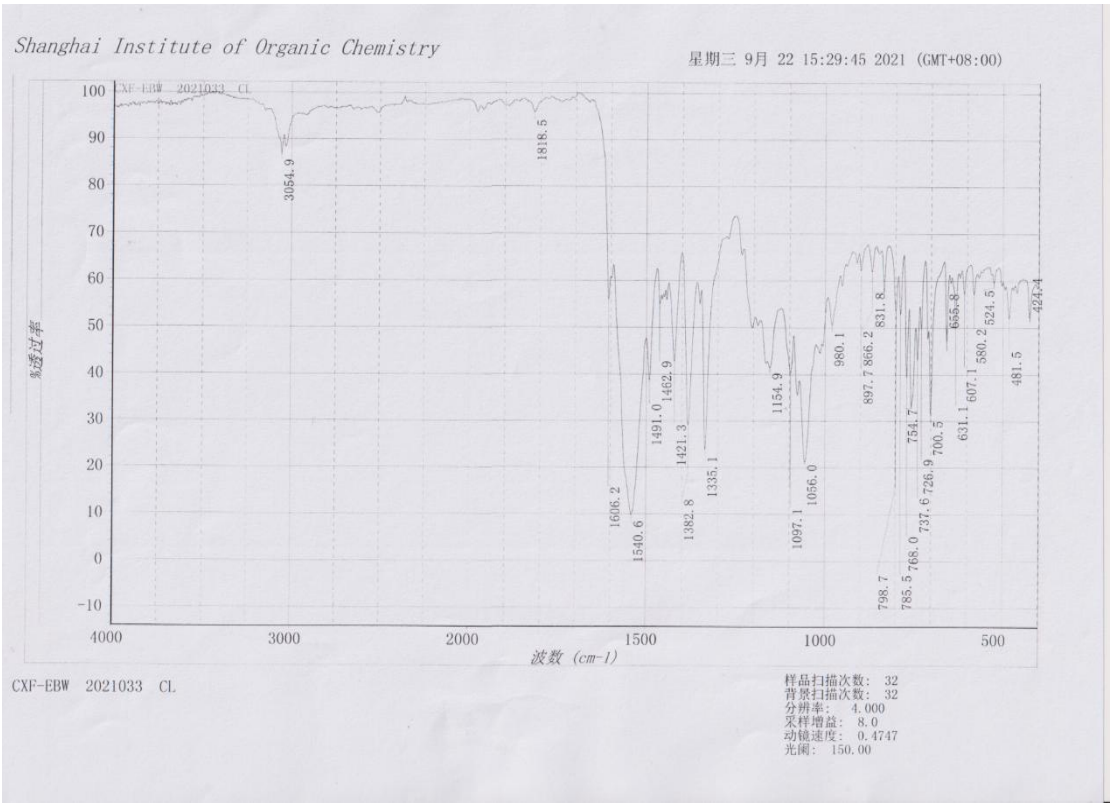

Fig. S24. FT-IR spectra of $DPFBF_2$.

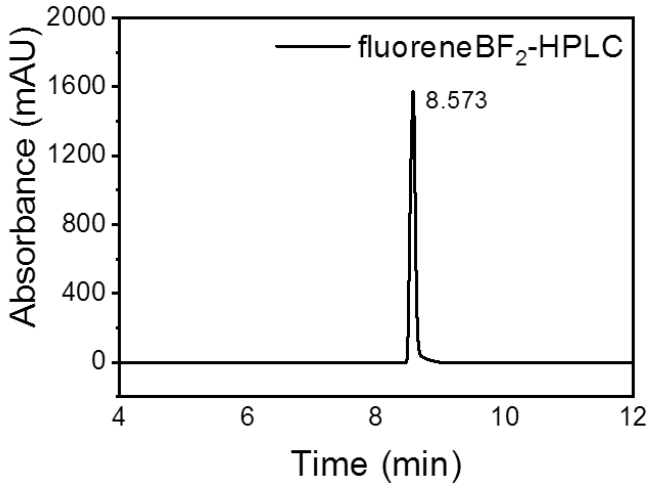

Fig. S25. HPLC spectrum of $DPEBF_2$. UV absorption was monitored at 376 nm.

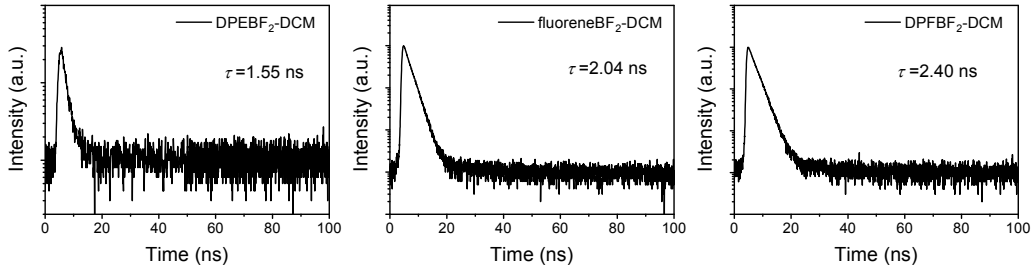

Fig. S26. The fluorescence decay profiles of BF_2bdk in dichloromethane.

Table S1. Photophysical data of BF_2bdk compounds at room temperature.

Entry	λ_{abs}/nm ($\varepsilon\times10^{-4}$/M^{-1}cm^{-1})	λ_{em}/nm	τ/ns
$DPEBF_2$ in dichloromethane	358 (3.05)	435	1.55
$DPEBF_2$ in ethyl acetate	346 (3.09)	395	1.51
$DPEBF_2$ in acetone	349 (3.25)	392	2.13
$DPEBF_2$ in tetrahydrofuran	347 (3.21)	396	1.62
$DPFBF_2$ in dichloromethane	384 (2.16)	440	2.40
$DPFBF_2$ in ethyl acetate	382 (1.27)	424	2.05
$DPFBF_2$ in acetone	382 (4.55)	438	2.52
$DPFBF_2$ in tetrahydrofuran	384 (2.78)	428	1.78

Table S2. Photophysical data of BF_2bdk-TPO-0.01% and BF_2bdk-TPO-0.5% powders at room temperature.

Entry	λ_F/nm	λ_P/nm
$DPEBF_2$-TPO-0.5%	412	486
$DPEBF_2$-TPO-0.01%	410	485
fluoreneBF_2-TPO-0.5%	440	528
fluoreneBF_2-TPO-0.01%	435	531
$DPFBF_2$-TPO-0.5%	463	531
$DPFBF_2$-TPO-0.01%	440	530
SpiroBF_2-TPO-0.5%	450	530
SpiroBF_2-TPO-0.01%	445	529

Table S3. Comparison of the S_1 and T_1 energy levels between TD-DFT results and experimental results.

Entry	BF_2bdk DT-DFT		BF_2bdk-0.5%-TPO melt-cast samples		BF_2bdk-0.5%-TPO powders		BF_2bdk-0.01%-TPO powders	
	S_1/eV	T_1/eV	S_1/eV	T_1/eV	S_1/eV	T_1/eV	S_1/eV	T_1/eV
$DPEBF_2$	4.01	2.83	2.99	2.55	3.00	2.55	3.02	2.56
$FluoreneBF_2$	3.40	2.45	2.79	2.36	2.82	2.35	2.85	2.33
$DPFBF_2$	3.31	2.65	2.80	2.37	2.68	2.34	2.82	2.34
$SpiroBF_2$	2.91	2.46	2.76	2.36	2.76	2.34	2.78	2.34

Table S4. Crystal data and structure refinement for d8v20637 ($DPEBF_2$).

Identification code	d8v20637	
Empirical formula	C16 H13 B F2 O3	
Formula weight	302.07	
Temperature	293(2) K	
Wavelength	0.71073 Å	
Crystal system	Orthorhombic	
Space group	P n m a	
Unit cell dimensions	a = 28.975(2) Å	α= 90°.
	b = 7.2581(5) Å	β= 90°.
	c = 6.7960(5) Å	γ = 90°.
Volume	1429.22(18) $Å^3$	
Z	4	
Density (calculated)	1.404 Mg/m^3	
Absorption coefficient	0.112 mm^{-1}	
F(000)	624	
Crystal size	0.200 x 0.140 x 0.110 mm^3	
Theta range for data collection	3.139 to 25.995°.	
Index ranges	-35<=h<=27, -8<=k<=8, -8<=l<=8	
Reflections collected	6622	
Independent reflections	1505 [R(int) = 0.0686]	
Completeness to theta = 25.242°	98.9 %	

Absorption correction	Semi-empirical from equivalents
Max. and min. transmission	0.7456 and 0.4799
Refinement method	Full-matrix least-squares on F^2
Data / restraints / parameters	1505 / 0 / 126
Goodness-of-fit on F^2	1.034
Final R indices [I>2sigma(I)]	R1 = 0.0452, wR2 = 0.1168
R indices (all data)	R1 = 0.0573, wR2 = 0.1296
Extinction coefficient	0.053(12)
Largest diff. peak and hole	0.198 and -0.181 e.$Å^{-3}$

Table S5. Atomic coordinates (x 10^4) and equivalent isotropic displacement parameters ($Å^2$ x10^3) for d8v20637 ($DPEBF_2$). U(eq) is defined as one third of the trace of the orthogonalized U^{ij} tensor.

	x	y	z	U(eq)
F(1)	4170(1)	5954(1)	9911(1)	69(1)
O(1)	3856(1)	7500	7237(2)	58(1)
O(2)	4685(1)	7500	7896(2)	61(1)
O(3)	6646(1)	7500	4142(3)	90(1)
C(1)	3548(1)	7500	4042(4)	65(1)
C(2)	3954(1)	7500	5378(3)	47(1)
C(3)	4399(1)	7500	4715(3)	50(1)
C(4)	4762(1)	7500	6030(3)	42(1)
C(5)	5250(1)	7500	5459(3)	42(1)
C(6)	5389(1)	7500	3500(3)	49(1)
C(7)	5852(1)	7500	2999(3)	51(1)
C(8)	6177(1)	7500	4476(3)	55(1)
C(9)	6048(1)	7500	6428(4)	67(1)
C(10)	5588(1)	7500	6911(3)	56(1)
C(11)	6818(1)	7500	2227(4)	62(1)
C(12)	6920(1)	5865(3)	1331(3)	73(1)
C(13)	7131(1)	5873(3)	-481(3)	77(1)
C(14)	7239(1)	7500	-1379(4)	74(1)
B(1)	4218(1)	7500	8786(4)	51(1)

Table S6. Bond lengths [Å] and angles [°] for d8v20637 ($DPEBF_2$).

F(1)-B(1)	1.3649(16)
O(1)-C(2)	1.295(3)
O(1)-B(1)	1.487(3)
O(2)-C(4)	1.288(2)
O(2)-B(1)	1.480(3)
O(3)-C(8)	1.378(3)
O(3)-C(11)	1.393(3)
C(1)-C(2)	1.487(3)
C(1)-H(1A)	0.9600
C(1)-H(1B)	0.9600
C(1)-H(1C)	0.9600
C(2)-C(3)	1.366(3)
C(3)-C(4)	1.381(3)
C(3)-H(3)	0.9300
C(4)-C(5)	1.464(3)
C(5)-C(6)	1.391(3)
C(5)-C(10)	1.391(3)
C(6)-C(7)	1.384(3)
C(6)-H(6)	0.9300
C(7)-C(8)	1.377(3)
C(7)-H(7)	0.9300
C(8)-C(9)	1.378(3)
C(9)-C(10)	1.374(3)
C(9)-H(9)	0.9300
C(10)-H(10)	0.9300
C(11)-C(12)#1	1.366(2)
C(11)-C(12)	1.366(2)
C(12)-C(13)	1.375(3)
C(12)-H(12)	0.9300
C(13)-C(14)	1.366(3)
C(13)-H(13)	0.9300
C(14)-C(13)#1	1.366(3)
C(14)-H(14)	0.9300
B(1)-F(1)#1	1.3648(16)
C(2)-O(1)-B(1)	122.37(18)
C(4)-O(2)-B(1)	124.19(18)

C(8)-O(3)-C(11)	120.32(18)
C(2)-C(1)-H(1A)	109.5
C(2)-C(1)-H(1B)	109.5
H(1A)-C(1)-H(1B)	109.5
C(2)-C(1)-H(1C)	109.5
H(1A)-C(1)-H(1C)	109.5
H(1B)-C(1)-H(1C)	109.5
O(1)-C(2)-C(3)	122.0(2)
O(1)-C(2)-C(1)	114.9(2)
C(3)-C(2)-C(1)	123.1(2)
C(2)-C(3)-C(4)	120.4(2)
C(2)-C(3)-H(3)	119.8
C(4)-C(3)-H(3)	119.8
O(2)-C(4)-C(3)	120.22(19)
O(2)-C(4)-C(5)	115.47(18)
C(3)-C(4)-C(5)	124.31(19)
C(6)-C(5)-C(10)	118.3(2)
C(6)-C(5)-C(4)	122.25(19)
C(10)-C(5)-C(4)	119.43(19)
C(7)-C(6)-C(5)	121.1(2)
C(7)-C(6)-H(6)	119.4
C(5)-C(6)-H(6)	119.4
C(8)-C(7)-C(6)	118.9(2)
C(8)-C(7)-H(7)	120.5
C(6)-C(7)-H(7)	120.5
C(7)-C(8)-O(3)	123.7(2)
C(7)-C(8)-C(9)	121.1(2)
O(3)-C(8)-C(9)	115.2(2)
C(10)-C(9)-C(8)	119.5(2)
C(10)-C(9)-H(9)	120.2
C(8)-C(9)-H(9)	120.2
C(9)-C(10)-C(5)	121.0(2)
C(9)-C(10)-H(10)	119.5
C(5)-C(10)-H(10)	119.5
C(12)#1-C(11)-C(12)	120.6(2)
C(12)#1-C(11)-O(3)	119.56(12)
C(12)-C(11)-O(3)	119.56(12)
C(11)-C(12)-C(13)	119.4(2)

C(11)-C(12)-H(12)	120.3
C(13)-C(12)-H(12)	120.3
C(14)-C(13)-C(12)	120.4(2)
C(14)-C(13)-H(13)	119.8
C(12)-C(13)-H(13)	119.8
C(13)#1-C(14)-C(13)	119.7(3)
C(13)#1-C(14)-H(14)	120.2
C(13)-C(14)-H(14)	120.2
F(1)#1-B(1)-F(1)	110.56(18)
F(1)#1-B(1)-O(2)	108.75(14)
F(1)-B(1)-O(2)	108.74(14)
F(1)#1-B(1)-O(1)	108.97(14)
F(1)-B(1)-O(1)	108.98(14)
O(2)-B(1)-O(1)	110.85(17)

Symmetry transformations used to generate equivalent atoms:
#1 x,-y+3/2,z

Table S7. Crystal data and structure refinement for mo_d8v20682_0m (fluoreneBF$_2$).

Identification code	mo_d8v20682_0m	
Empirical formula	C19 H17 B F2 O2	
Formula weight	326.13	
Temperature	293(2) K	
Wavelength	0.71073 Å	
Crystal system	Monoclinic	
Space group	P 21/m	
Unit cell dimensions	a = 8.1515(6) Å	α= 90°.
	b = 7.1248(6) Å	β=103.612(2)°.
	c = 14.2590(11) Å	γ= 90°.
Volume	804.87(11) Å^3	
Z	2	
Density (calculated)	1.346 Mg/m^3	
Absorption coefficient	0.100 mm^{-1}	
F(000)	340	
Crystal size	0.200 x 0.150 x 0.110 mm^3	

Theta range for data collection	2.644 to 25.996°.
Index ranges	-10<=h<=10, -8<=k<=8, -15<=l<=17
Reflections collected	12022
Independent reflections	1695 [R(int) = 0.0628]
Completeness to theta = 25.242°	98.9 %
Absorption correction	Semi-empirical from equivalents
Max. and min. transmission	0.7456 and 0.5089
Refinement method	Full-matrix least-squares on F^2
Data / restraints / parameters	1695 / 0 / 142
Goodness-of-fit on F^2	1.054
Final R indices [I>2sigma(I)]	R1 = 0.0487, wR2 = 0.1253
R indices (all data)	R1 = 0.0568, wR2 = 0.1334
Extinction coefficient	0.11(3)
Largest diff. peak and hole	0.302 and -0.273 e.Å^{-3}

Table S8. Atomic coordinates (x 10^4) and equivalent isotropic displacement parameters (Å^{2}x 10^3) for mo_d8v20682_0m (fluoreneBF$_2$). U(eq) is defined as one third of the trace of the orthogonalized U^{ij} tensor.

	x	y	z	U(eq)
F(1)	2122(2)	5927(3)	8594(1)	128(1)
O(1)	3071(2)	7500	7424(1)	59(1)
O(2)	4590(3)	7500	9119(1)	77(1)
C(1)	1236(2)	7500	3646(1)	38(1)
C(2)	2083(3)	7500	2803(1)	41(1)
C(3)	1337(3)	7500	1824(2)	57(1)
C(4)	2368(4)	7500	1175(2)	64(1)
C(5)	4099(4)	7500	1491(2)	60(1)
C(6)	4863(3)	7500	2466(2)	49(1)
C(7)	3838(3)	7500	3118(1)	38(1)
C(8)	4267(2)	7500	4175(1)	34(1)
C(9)	5823(3)	7500	4827(2)	42(1)

C(10)	5876(3)	7500	5800(2)	43(1)
C(11)	4406(3)	7500	6138(1)	36(1)
C(12)	2833(2)	7500	5475(1)	35(1)
C(13)	2772(2)	7500	4496(1)	33(1)
C(14)	140(2)	5749(2)	3639(1)	51(1)
C(15)	4501(3)	7500	7182(1)	40(1)
C(16)	5990(3)	7500	7881(2)	56(1)
C(17)	5978(4)	7500	8842(2)	56(1)
C(18)	7556(4)	7500	9626(2)	82(1)
B(1)	2925(4)	7500	8440(2)	63(1)

Table S9. Bond lengths [Å] and angles [°] for mo_d8v20682_0m (fluoreneBF$_2$).

F(1)-B(1)	1.342(2)
O(1)-C(15)	1.291(3)
O(1)-B(1)	1.483(3)
O(2)-C(17)	1.283(3)
O(2)-B(1)	1.470(4)
C(1)-C(2)	1.521(3)
C(1)-C(13)	1.524(3)
C(1)-C(14)	1.5333(19)
C(1)-C(14)#1	1.5333(19)
C(2)-C(3)	1.384(3)
C(2)-C(7)	1.395(3)
C(3)-C(4)	1.389(3)
C(3)-H(3)	0.9300
C(4)-C(5)	1.377(4)
C(4)-H(4)	0.9300
C(5)-C(6)	1.383(3)
C(5)-H(5)	0.9300
C(6)-C(7)	1.390(3)
C(6)-H(6)	0.9300
C(7)-C(8)	1.464(3)
C(8)-C(9)	1.385(3)
C(8)-C(13)	1.399(3)
C(9)-C(10)	1.378(3)

C(9)-H(9)	0.9300
C(10)-C(11)	1.392(3)
C(10)-H(10)	0.9300
C(11)-C(12)	1.403(3)
C(11)-C(15)	1.472(3)
C(12)-C(13)	1.385(3)
C(12)-H(12)	0.9300
C(14)-H(14A)	0.9600
C(14)-H(14B)	0.9600
C(14)-H(14C)	0.9600
C(15)-C(16)	1.378(3)
C(16)-C(17)	1.372(3)
C(16)-H(16)	0.9300
C(17)-C(18)	1.492(3)
C(18)-H(18A)	0.9600
C(18)-H(18B)	0.9600
C(18)-H(18C)	0.9600
B(1)-F(1)#1	1.342(2)
C(15)-O(1)-B(1)	123.16(19)
C(17)-O(2)-B(1)	122.83(19)
C(2)-C(1)-C(13)	100.85(15)
C(2)-C(1)-C(14)	111.52(10)
C(13)-C(1)-C(14)	111.96(10)
C(2)-C(1)-C(14)#1	111.52(10)
C(13)-C(1)-C(14)#1	111.96(10)
C(14)-C(1)-C(14)#1	108.90(17)
C(3)-C(2)-C(7)	119.96(19)
C(3)-C(2)-C(1)	128.55(19)
C(7)-C(2)-C(1)	111.48(16)
C(2)-C(3)-C(4)	118.7(2)
C(2)-C(3)-H(3)	120.6
C(4)-C(3)-H(3)	120.6
C(5)-C(4)-C(3)	121.1(2)
C(5)-C(4)-H(4)	119.5
C(3)-C(4)-H(4)	119.5
C(4)-C(5)-C(6)	120.9(2)
C(4)-C(5)-H(5)	119.6
C(6)-C(5)-H(5)	119.6

C(5)-C(6)-C(7)	118.3(2)
C(5)-C(6)-H(6)	120.9
C(7)-C(6)-H(6)	120.9
C(6)-C(7)-C(2)	121.10(19)
C(6)-C(7)-C(8)	130.8(2)
C(2)-C(7)-C(8)	108.12(16)
C(9)-C(8)-C(13)	120.64(17)
C(9)-C(8)-C(7)	130.60(18)
C(13)-C(8)-C(7)	108.76(17)
C(10)-C(9)-C(8)	118.89(19)
C(10)-C(9)-H(9)	120.6
C(8)-C(9)-H(9)	120.6
C(9)-C(10)-C(11)	121.52(19)
C(9)-C(10)-H(10)	119.2
C(11)-C(10)-H(10)	119.2
C(10)-C(11)-C(12)	119.44(18)
C(10)-C(11)-C(15)	120.33(18)
C(12)-C(11)-C(15)	120.23(18)
C(13)-C(12)-C(11)	119.29(18)
C(13)-C(12)-H(12)	120.4
C(11)-C(12)-H(12)	120.4
C(12)-C(13)-C(8)	120.21(17)
C(12)-C(13)-C(1)	129.00(17)
C(8)-C(13)-C(1)	110.78(16)
C(1)-C(14)-H(14A)	109.5
C(1)-C(14)-H(14B)	109.5
H(14A)-C(14)-H(14B)	109.5
C(1)-C(14)-H(14C)	109.5
H(14A)-C(14)-H(14C)	109.5
H(14B)-C(14)-H(14C)	109.5
O(1)-C(15)-C(16)	120.22(19)
O(1)-C(15)-C(11)	115.75(18)
C(16)-C(15)-C(11)	124.0(2)
C(17)-C(16)-C(15)	120.7(2)
C(17)-C(16)-H(16)	119.6
C(15)-C(16)-H(16)	119.6
O(2)-C(17)-C(16)	121.4(2)
O(2)-C(17)-C(18)	115.9(2)

C(16)-C(17)-C(18)	122.7(3)
C(17)-C(18)-H(18A)	109.5
C(17)-C(18)-H(18B)	109.5
H(18A)-C(18)-H(18B)	109.5
C(17)-C(18)-H(18C)	109.5
H(18A)-C(18)-H(18C)	109.5
H(18B)-C(18)-H(18C)	109.5
F(1)#1-B(1)-F(1)	113.4(3)
F(1)#1-B(1)-O(2)	107.65(16)
F(1)-B(1)-O(2)	107.65(16)
F(1)#1-B(1)-O(1)	108.29(14)
F(1)-B(1)-O(1)	108.29(14)
O(2)-B(1)-O(1)	111.7(2)

Symmetry transformations used to generate equivalent atoms:
#1 x,-y+3/2,z

Table S10. Crystal data and structure refinement for mo_d8v20638_0m (SpiroBF$_2$).

Identification code	mo_d8v20638_0m	
Empirical formula	C29 H19 B F2 O2	
Formula weight	448.25	
Temperature	293.4 K	
Wavelength	0.71073 Å	
Crystal system	Monoclinic	
Space group	P 1 21/n 1	
Unit cell dimensions	a = 10.0422(5) Å	α= 90°.
	b = 18.3455(7) Å	β= 99.116(2)°.
	c = 14.3713(7) Å	γ= 90°.
Volume	2614.2(2) Å^3	
Z	4	
Density (calculated)	1.139 Mg/m^3	
Absorption coefficient	0.080 mm^{-1}	
F(000)	928	
Crystal size	0.2 x 0.16 x 0.12 mm^3	

Theta range for data collection	2.565 to 27.484°.
Index ranges	-12<=h<=13, -23<=k<=23, -18<=l<=14
Reflections collected	14395
Independent reflections	5917 [R(int) = 0.0432]
Completeness to theta = 25.242°	99.2 %
Absorption correction	Semi-empirical from equivalents
Max. and min. transmission	0.7456 and 0.5811
Refinement method	Full-matrix least-squares on F^2
Data / restraints / parameters	5917 / 0 / 308
Goodness-of-fit on F^2	1.016
Final R indices [I>2sigma(I)]	R1 = 0.0561, wR2 = 0.1552
R indices (all data)	R1 = 0.0958, wR2 = 0.1866
Extinction coefficient	n/a
Largest diff. peak and hole	0.171 and -0.167 e.Å^{-3}

Table S11. Atomic coordinates (x 10^4) and equivalent isotropic displacement parameters (Å^{2}x 10^3) for mo_d8v20638_0m (SpiroBF$_2$). U(eq) is defined as one third of the trace of the orthogonalized U^{ij} tensor.

	x	y	z	U(eq)
F(1)	2481(1)	5510(1)	4187(1)	86(1)
F(2)	2584(2)	5184(1)	2691(1)	102(1)
O(1)	3471(1)	4415(1)	3904(1)	76(1)
O(2)	4518(1)	5584(1)	3646(1)	72(1)
C(1)	4697(3)	3324(1)	4181(2)	80(1)
C(2)	4641(2)	4114(1)	3941(1)	58(1)
C(3)	5739(2)	4506(1)	3793(2)	59(1)
C(4)	5666(2)	5253(1)	3676(1)	50(1)
C(5)	6829(2)	5721(1)	3614(1)	50(1)
C(6)	8114(2)	5428(1)	3633(2)	65(1)
C(7)	9211(2)	5865(1)	3567(2)	69(1)
C(8)	9023(2)	6616(1)	3494(1)	52(1)

C(9)	9982(2)	7208(1)	3425(1)	54(1)
C(10)	11360(2)	7194(1)	3407(2)	72(1)
C(11)	12032(2)	7850(1)	3364(2)	80(1)
C(12)	11351(2)	8504(1)	3338(2)	75(1)
C(13)	9974(2)	8520(1)	3352(1)	63(1)
C(14)	9290(2)	7866(1)	3397(1)	51(1)
C(15)	7801(2)	7746(1)	3438(1)	48(1)
C(16)	7746(2)	6915(1)	3492(1)	47(1)
C(17)	6648(2)	6479(1)	3539(1)	49(1)
C(18)	6838(2)	8065(1)	2614(1)	52(1)
C(19)	6806(2)	7940(1)	1663(2)	65(1)
C(20)	5805(2)	8296(1)	1032(2)	79(1)
C(21)	4886(3)	8751(1)	1351(2)	83(1)
C(22)	4911(2)	8870(1)	2294(2)	76(1)
C(23)	5905(2)	8528(1)	2934(2)	61(1)
C(24)	6193(2)	8556(1)	3963(2)	65(1)
C(25)	5591(3)	8941(1)	4623(2)	93(1)
C(26)	6117(4)	8882(2)	5559(2)	109(1)
C(27)	7210(4)	8449(2)	5854(2)	96(1)
C(28)	7813(3)	8060(1)	5216(2)	72(1)
C(29)	7306(2)	8117(1)	4273(1)	55(1)
B(1)	3229(2)	5178(1)	3596(2)	68(1)

Table S12. Bond lengths [Å] and angles [°] for mo_d8v20638_0m (SpiroBF$_2$).

F(1)-B(1)	1.363(3)
F(2)-B(1)	1.359(3)
O(1)-C(2)	1.291(2)
O(1)-B(1)	1.477(3)
O(2)-C(4)	1.297(2)
O(2)-B(1)	1.485(3)
C(1)-H(1A)	0.9600
C(1)-H(1B)	0.9600
C(1)-H(1C)	0.9600
C(1)-C(2)	1.490(3)
C(2)-C(3)	1.360(3)
C(3)-H(3)	0.9300

C(3)-C(4)	1.382(2)
C(4)-C(5)	1.463(2)
C(5)-C(6)	1.395(2)
C(5)-C(17)	1.405(2)
C(6)-H(6)	0.9300
C(6)-C(7)	1.379(3)
C(7)-H(7)	0.9300
C(7)-C(8)	1.393(3)
C(8)-C(9)	1.465(2)
C(8)-C(16)	1.394(2)
C(9)-C(10)	1.389(3)
C(9)-C(14)	1.391(3)
C(10)-H(10)	0.9300
C(10)-C(11)	1.385(3)
C(11)-H(11)	0.9300
C(11)-C(12)	1.378(3)
C(12)-H(12)	0.9300
C(12)-C(13)	1.387(3)
C(13)-H(13)	0.9300
C(13)-C(14)	1.390(2)
C(14)-C(15)	1.522(2)
C(15)-C(16)	1.527(2)
C(15)-C(18)	1.522(3)
C(15)-C(29)	1.530(2)
C(16)-C(17)	1.372(2)
C(17)-H(17)	0.9300
C(18)-C(19)	1.381(3)
C(18)-C(23)	1.395(3)
C(19)-H(19)	0.9300
C(19)-C(20)	1.405(3)
C(20)-H(20)	0.9300
C(20)-C(21)	1.376(4)
C(21)-H(21)	0.9300
C(21)-C(22)	1.368(4)
C(22)-H(22)	0.9300
C(22)-C(23)	1.395(3)
C(23)-C(24)	1.462(3)
C(24)-C(25)	1.395(3)

C(24)-C(29)	1.393(3)
C(25)-H(25)	0.9300
C(25)-C(26)	1.369(4)
C(26)-H(26)	0.9300
C(26)-C(27)	1.366(4)
C(27)-H(27)	0.9300
C(27)-C(28)	1.376(3)
C(28)-H(28)	0.9300
C(28)-C(29)	1.374(3)

C(2)-O(1)-B(1)	121.51(16)
C(4)-O(2)-B(1)	122.08(15)
H(1A)-C(1)-H(1B)	109.5
H(1A)-C(1)-H(1C)	109.5
H(1B)-C(1)-H(1C)	109.5
C(2)-C(1)-H(1A)	109.5
C(2)-C(1)-H(1B)	109.5
C(2)-C(1)-H(1C)	109.5
O(1)-C(2)-C(1)	115.19(17)
O(1)-C(2)-C(3)	121.51(17)
C(3)-C(2)-C(1)	123.27(19)
C(2)-C(3)-H(3)	119.5
C(2)-C(3)-C(4)	120.96(18)
C(4)-C(3)-H(3)	119.5
O(2)-C(4)-C(3)	119.81(16)
O(2)-C(4)-C(5)	115.95(15)
C(3)-C(4)-C(5)	124.20(17)
C(6)-C(5)-C(4)	121.17(15)
C(6)-C(5)-C(17)	119.43(16)
C(17)-C(5)-C(4)	119.39(15)
C(5)-C(6)-H(6)	119.3
C(7)-C(6)-C(5)	121.40(17)
C(7)-C(6)-H(6)	119.3
C(6)-C(7)-H(7)	120.6
C(6)-C(7)-C(8)	118.75(17)
C(8)-C(7)-H(7)	120.6
C(7)-C(8)-C(9)	130.90(17)
C(7)-C(8)-C(16)	120.22(16)

C(16)-C(8)-C(9)	108.88(16)
C(10)-C(9)-C(8)	131.05(18)
C(10)-C(9)-C(14)	120.65(18)
C(14)-C(9)-C(8)	108.28(16)
C(9)-C(10)-H(10)	120.7
C(11)-C(10)-C(9)	118.6(2)
C(11)-C(10)-H(10)	120.7
C(10)-C(11)-H(11)	119.5
C(12)-C(11)-C(10)	121.0(2)
C(12)-C(11)-H(11)	119.5
C(11)-C(12)-H(12)	119.7
C(11)-C(12)-C(13)	120.6(2)
C(13)-C(12)-H(12)	119.7
C(12)-C(13)-H(13)	120.5
C(12)-C(13)-C(14)	119.0(2)
C(14)-C(13)-H(13)	120.5
C(9)-C(14)-C(15)	111.29(15)
C(13)-C(14)-C(9)	120.17(18)
C(13)-C(14)-C(15)	128.53(18)
C(14)-C(15)-C(16)	100.94(14)
C(14)-C(15)-C(18)	114.92(14)
C(14)-C(15)-C(29)	114.18(15)
C(16)-C(15)-C(29)	112.61(14)
C(18)-C(15)-C(16)	113.62(13)
C(18)-C(15)-C(29)	101.16(14)
C(8)-C(16)-C(15)	110.61(15)
C(17)-C(16)-C(8)	121.12(15)
C(17)-C(16)-C(15)	128.27(16)
C(5)-C(17)-H(17)	120.5
C(16)-C(17)-C(5)	119.05(16)
C(16)-C(17)-H(17)	120.5
C(19)-C(18)-C(15)	128.10(17)
C(19)-C(18)-C(23)	121.07(19)
C(23)-C(18)-C(15)	110.83(17)
C(18)-C(19)-H(19)	121.2
C(18)-C(19)-C(20)	117.6(2)
C(20)-C(19)-H(19)	121.2
C(19)-C(20)-H(20)	119.5

C(21)-C(20)-C(19)	121.1(2)
C(21)-C(20)-H(20)	119.5
C(20)-C(21)-H(21)	119.4
C(22)-C(21)-C(20)	121.3(2)
C(22)-C(21)-H(21)	119.4
C(21)-C(22)-H(22)	120.7
C(21)-C(22)-C(23)	118.7(2)
C(23)-C(22)-H(22)	120.7
C(18)-C(23)-C(22)	120.3(2)
C(18)-C(23)-C(24)	108.61(18)
C(22)-C(23)-C(24)	131.1(2)
C(25)-C(24)-C(23)	132.0(2)
C(29)-C(24)-C(23)	108.87(17)
C(29)-C(24)-C(25)	119.1(2)
C(24)-C(25)-H(25)	120.4
C(26)-C(25)-C(24)	119.1(3)
C(26)-C(25)-H(25)	120.4
C(25)-C(26)-H(26)	119.4
C(27)-C(26)-C(25)	121.1(3)
C(27)-C(26)-H(26)	119.4
C(26)-C(27)-H(27)	119.6
C(26)-C(27)-C(28)	120.7(3)
C(28)-C(27)-H(27)	119.6
C(27)-C(28)-H(28)	120.5
C(29)-C(28)-C(27)	119.0(2)
C(29)-C(28)-H(28)	120.5
C(24)-C(29)-C(15)	110.48(17)
C(28)-C(29)-C(15)	128.64(19)
C(28)-C(29)-C(24)	120.88(19)
F(1)-B(1)-O(1)	108.49(19)
F(1)-B(1)-O(2)	107.99(19)
F(2)-B(1)-F(1)	111.5(2)
F(2)-B(1)-O(1)	109.0(2)
F(2)-B(1)-O(2)	108.8(2)
O(1)-B(1)-O(2)	111.06(18)

Symmetry transformations used to generate equivalent atoms: